CHAOS CONTROL USING A GENERALIZED EXTENDED TIME-DELAYED FEEDBACK METHOD: APPLICATION TO A NONLINEAR PENDULUM

Arthur Rodrigues Queiroz

Master's Dissertation

Mechanical Sciences

UNIVERSIDADE DE BRASÍLIA

Faculdade de Tecnologia

Departamento de Engenharia Mecânica

UNIVERSIDADE DE BRASÍLIA
FACULDADE DE TECNOLOGIA
DEPARTAMENTO DE ENGENHARIA MECÂNICA

CHAOS CONTROL USING A GENERALIZED EXTENDED TIME-DELAYED FEEDBACK METHOD: APPLICATION TO A NONLINEAR PENDULUM

Arthur Rodrigues Queiroz

Orientadora: Aline Souza de Paula, Dr. Univ (ENM/UnB)

DISSERTAÇÃO DE MESTRADO

PUBLICAÇÃO: ENM.DM - XXX.XXX

BRASÍLIA/DF: 01 de dezembro de 2023

UNIVERSIDADE DE BRASÍLIA
FACULDADE DE TECNOLOGIA
DEPARTAMENTO DE ENGENHARIA MECÂNICA

Chaos Control Using a Generalized Extended Time-Delayed Feedback Method: Application to a Nonlinear Pendulum

Arthur Rodrigues Queiroz

DISSERTAÇÃO DE MESTRADO SUBMETIDA AO DEPARTAMENTO DE ENGENHARIA MECÂNICA DA FACULDADE DE TECNOLOGIA DA UNIVERSIDADE DE BRASÍLIA COMO PARTE DOS REQUISITOS PARCIAIS PARA A OBTENÇÃO DO GRAU DE MESTRE EM CIÊNCIAS MECÂNICAS.

APROVADA POR:

Aline Souza de Paula, Dr. Univ (ENM/UnB)
(Orientadora)

Rafael Gabler Gontijo, Dr. Univ (ENM/UnB)
(Examinadora Interna)

Americo Barbosa da Cunha Junior, Dr. Univ (IME/UERJ)
(Examinadora Externa)

BRASÍLIA/DF, 01 DE DEZEMBRO DE 2023.

FICHA CATALOGRÁFICA

Queiroz, A. R.
Chaos Control Using a Generalized Extended Time-Delayed Feedback Method: Application to a Nonlinear Pendulum
[Distrito Federal] 2023.
xvii, 84p. (ENM/FT/UnB, Mestre, Ciências Mecânicas, 2023.
Dissertação de Mestrado - Universidade de Brasília.
Faculdade de Tecnologia.
Departamento de Engenharia Mecânica.
Palavras-chave:
1. Chaos Control 2. Nonlinear Dynamics
3. Pendulum 4. ETDF
I. ENM/FT/UnB II. Título (série)

REFERÊNCIA BIBLIOGRÁFICA

Queiroz, A. R.(2023). Chaos Control Using a Generalized Extended Time-Delayed Feedback Method: Application to a Nonlinear Pendulum. Dissertação de Mestrado, Publicação ENM.DM - XXX.XXX, Departamento de Engenharia Mecânica, Universidade de Brasília, Brasília, Distrito Federal, xvii, 84p.

CESSÃO DE DIREITOS

NOME DO AUTOR: Arthur Rodrigues Queiroz.

TÍTULO DA DISSERTAÇÃO DE MESTRADO: Chaos Control Using a Generalized Extended Time-Delayed Feedback Method: Application to a Nonlinear Pendulum.

GRAU / ANO: MESTRE / 2023

Arthur Rodrigues Queiroz

À memória de Lauro Rodrigues.

Abstract

CHAOS CONTROL USING A GENERALIZED EXTENDED TIME-DELAYED FEEDBACK METHOD: APPLICATION TO A NONLINEAR PENDULUM

Author: Arthur Rodrigues Queiroz

Supervisor: Aline Souza de Paula, Dr. Univ (ENM/UnB)

Graduate Program in Mechanical Sciences

Brasília, 2023

Chaos exhibits a richness of periodic patterns with great sensitivity to small disturbances. Chaos control exploits this sensitivity and, with small disturbances, stabilizes one of its countless trajectories. This work explores a generalization of the Extended Time-Delayed Feedback (ETDF) method to stabilize unstable periodic orbits (UPOs). This generalization considers the complete matrix gain **K** instead of the conventional scalar gain approach. A nonlinear pendulum is chosen as the system for applying the method. Three UPOs, with periodicities 1, 2 and 3, are selected to evaluate the control strategy. The controller gains are evaluated by determining stability through the largest Lyapunov exponent. The matrix term K_{12} consistently increases system instability across all evaluated cases, leading to its exclusion for control purposes. Cases involving two parameters with K_{11} and K_{22}, as well as K_{21} and K_{22}, and the three-parameter case comprising K_{11}, K_{21} and K_{22} are considered. All combinations considered reveal a broader region of stability for the system compared to the scalar-base approach, but generally with similar magnitudes for the Lyapunov exponent. The actuation of the controller and the corresponding energy consumption are compared for each stabilization scenario. The possibility of migration between the selected UPOs is also evaluated. The results showed good flexibility when using the matrix **K**, prioritizing the system's needs, whether with smaller actuations or energy consumption. In the control implementations without K_{21}, it is possible to transition between all orbits according to the control rule, whereas in those that considered this parameter, the stabilization of the period-1 UPO is not achieved.

Keywords: Chaos Control; Nonlinear Dynamics; Pendulum; ETDF

Resumo

CONTROLE DE CAOS UTILIZANDO MÉTODO DA REALIMENTAÇÃO COM ESTADOS DEFASADOS ESTENDIDOS GENERALIZADO: APLICAÇÃO A UM PÊNDULO NÃO-LINEAR

Autor: Arthur Rodrigues Queiroz

Orientadora: Aline Souza de Paula, Dr. Univ (ENM/UnB)

Programa de Pós Graduação em Ciências Mecânicas

Brasília, 01 de dezembro de 2023

O caos exibe uma riqueza da padrões periódicos com grande sensibilidade a pequenas perturbações. O controle de caos explora essa sensibilidade, e com pequenas perturbações, estabiliza uma de suas inúmeras trajetórias. Este trabalho explora uma generalização do método da Realimentação com Estados Defasados Estendidos (ETDF) para estabilizar órbitas periódicas instáveis (OPIs). Essa generalização considera a matriz de ganhos **K** completa ao invés da abordagem tradicional com ganho escalar. Um pêndulo não-linear é considerado como sistema para aplicação do método. São selecionadas 3 OPIs para controle, de periodicidades 1, 2 e 3. A determinação dos ganhos do controlador é feita através da estabilidade das OPIs utilizando o expoente de Lyapunov máximo. O ganho K_{12} da matriz aumenta a instabilidade do sistema em todos os casos avaliados, sendo desconsiderado. É considerados casos com 2 ganhos combinados, sendo K_{11} e K_{22}, e K_{21} e K_{22}, e o caso com três ganhos K_{11}, K_{21} e K_{22}. Todas os casos considerados revelam uma maior região de estabilidade quando comparados ao caso escalar, mas com valores de magnitudes semelhantes do expoente de Lyapunov. O desempenho do controlador é avaliado pelas magnitudes de atuação e energia consumida. A possiblidade de migração entre as OPIs selecionadas também é avaliada, mostrando boa flexibilidade de resposta, sendo possível priorizar menores atuações ou consumo energético. Nas implementações do controle sem K_{21}, é possível transitar entre todas as órbitas conforme a regra de controle, enquanto nas que consideraram esse ganho, a estabilização da OPI de período-1 não é alcançada.

Palavras-chaves: Controle de Caos; Dinâmica Não-linear; Pêndulo; ETDF.

Summary

List of Figures

List of Tables

Acronyms

DDE Delayed Differential Equation. 19, 20

ETDF Extended Time-Delayed Feedback. v, 3, 4, 9–11, 18, 19, 28, 44, 53, 58, 59

ODE Ordinary Differential Equation. 2, 19, 20

OGY Ott-Grebogy-York. 3, 6–8

SC semi-continuous. 7, 8

TDF Time-Delayed Feedback. 3, 6, 8–10, 18

UPO unstable periodic orbit. v, 2–4, 6, 8–11, 15–20, 27–29, 32, 33, 37, 38, 40, 42, 44, 46, 47, 49, 50, 52, 54–59

List of Algorithms

1 Introduction

Natural phenomena are full of nonlinearities in a manner that linear behavior is rare in nature. One of the possibilities of a nonlinear system response is the chaotic behavior. This response strongly depends on initial conditions, which makes small perturbations produce massive, disproportional effects. This sensitivity to initial conditions is such that there is always uncertainty about the system's future state due to numerical and measure limitations. Furthermore, the chaotic response is composed of a dense and infinite set of unstable periodic orbits (UPO). This richness makes chaos of particular interest in dynamical system design, conferring flexibility that can be observed by quick changes among different kinds of responses (LINDNER; DITTO, 1995). Moreover, chaos has an ergodic characteristic, which implies that the system will visit all parts of the space in which it is immersed.

For a long time, the study of chaos was left aside; the chaotic response was hard to predict and analyze and, therefore, unwanted. Due to its richness and sensitivity to disturbances, it was commonly confused with randomness. However, this thought/perception was proven incorrect. While stochastic behavior follows a probability function, chaos, although unpredictable, occurs in completely deterministic systems (KING; STEWART, 1991). Chaotic dynamics gained more interest from researchers after 1963, with Lorentz and his studies on the unpredictability of meteorological models (LORENZ, 1963). Lorentz noticed that even with a simple system of nonlinear ODEs, a slight variation in its initial conditions caused the system to move towards a completely different response. Subsequently, chaotic behavior was verified in several simple dynamic systems, developing chaos theory research in several areas of knowledge, among them mechanical systems (SHAW; RAND, 1989), medicine (SKINNER et al., 1992; WEST, 2012), chemistry (SCHÖLL; SCHUSTER, 2008; GIBB, 2009; RÖSSLER, 1981), ecology (HASTINGS et al., 1993; WORSTER, 1990), astronomy (ZEEBE; LOURENS, 2019; LASKAR et al., 2011; LECAR et al., 2001), and communication (ABEL; SCHWARZ, 2002). Recently, chaos research has gone beyond the mere characterization of behavior, looking for interventions to prevent its emergence or even, in some situations, seeking it.

Chaos is often unwanted and can harm the system; chaos control can be quite promising in these situations. For example, in the control of cardiac arrhythmia (LOUNIS; BOUKABOU; SOUKKOU, 2020; FERREIRA; SAVI; PAULA, 2014; GARFINKEL

et al., 1992), energy generation systems based on harnessing vibrational energy (MOHAMMADPOUR et al., 2023; TAN et al., 2021; KUMAR; ALI; AROCKIARAJAN, 2016; DEHGHANI; KHANLO, 2019; BARBOSA et al., 2015), preventing chaos in crystal growth to prevent structure failures (ZHOU; GREBOGI; REN, 2021), increase comfort in vehicles on uneven terrain (LITAK et al., 2008).

On the other hand, the chaotic response can also be desirable, for example, in space navigation where utilizing control to exploit the richness of trajectories enables low fuel consumption (CHEN; YU, 2003). Search methods of optimization algorithms can take advantage of chaos as input for its search algorithms, taking advantage of their ergodic character to avoid local minima (FENG et al., 2017; YANG; LI; CHENG, 2007; LI et al., 2006). The chaotic broad spectrum has high mixing performance in solid-liquid systems (GU et al., 2017). Anti-control techniques to generate a chaotic response archive better results in the vibration compaction (WANG; CHAU, 2008). Furthermore, chaos is used in commercial fiber-optic data links to improve its transmission rate (ARGYRIS et al., 2005).

The main idea of chaos control is to take advantage of the big sensitivity of the system to small disturbances, to stabilize one of the infinite UPO immersed in the chaotic response. The theoretical possibility of stabilizing any of the UPO can provide the system great flexibility. In addition, the sensitivity to small disturbances implies a stabilization with small perturbations associated with low energy consumption. The Ott-Grebogy-York (OGY) method (OTT; GREBOGI; YORKE, 1990) was a pioneer in chaos control. This discrete method applies a perturbation in a specific control section to stabilize the UPO. The first continuous method was the Time-Delayed Feedback (TDF), proposed by Pyragas (1992), where disturbance is continuously applied to the system based on a delayed and the actual states of the system. Subsequently, Socolar, Sukow & Gauthier (1994) proposed the Extended Time-Delayed Feedback (ETDF) where the control action is based on several delayed states of the system.

The nonlinear pendulum has been vastly used as the base for numerical simulations in chaos control control methods. This pendulum was previously studied by (BLACKBURN; BAKER, 1998), (FRANCA; SAVI, 2001), (DESERIO, 2003), (PINTO; SAVI, 2003), (PEREIRA-PINTO; FERREIRA; SAVI, 2004), (SAVI, 2006), (PAULA; SAVI; PEREIRA-PINTO, 2006), (BESSA; PAULA; SAVI, 2009),(PAULA; SAVI, 2009a), (PAULA; SAVI, 2011), (BESSA; PAULA; SAVI, 2014), (PAULA; SAVI, 2015), (COSTA; SAVI, 2017), (COSTA; SAVI, 2018). These studies evaluated the chaotic dynamics present in the system, applying and developing control methods. As a contribution of the present work, there is the publication Queiroz, Paula & Savi (2023).

1.1 Objectives

In the existing literature, the prevailing approach to the ETDF method often treats the gain matrix $\mathbf{K}$ as a scalar K. This dissertation aims to investigate a generalization of the Extended Time-Delayed Feedback method for chaos control by considering the complete gain matrix $\mathbf{K}$ instead of the conventional scalar approach. In the present study, the influence of the complete matrix is evaluated. The gains are chosen based on the values of the maximum Lyapunov exponents. Control performance is evaluated for different values of $\mathbf{K}$ by means of control actuation magnitudes and energy consumption.

1.2 Text Organization

This dissertation is divided into 7 chapters. The first chapter presents an introduction to this work, the objectives, methodology, and organization. Chapter 2 brings a literature review about studies of chaos on mechanical systems and chaos control. Chapter 3 presents the nonlinear dynamics analysis tools used in this work and the Extended Time-Delayed Feedback (ETDF) chaos control method. Chapter 4 aims to present the studied nonlinear pendulum, the mathematical modeling of the control on it, and a brief analysis of its dynamics without control.

Chapter 5 presents the first stage of the control. This chapter identifies the UPOs of interest, and the Lyapunov exponent is calculated. The results of the learning stage are analyzed. Chapter 6 is presented and analyzes the results of the control. This chapter compares maximum actuation, energy, and time until stabilization. Finally, Chapter 7 presents the conclusions of this dissertation and proposes future studies.

2 Literature review

One of the first names to deal with chaos was Henri Poincaré in his work Poincaré (1890). Evaluating the three-body problem, he realized the existence of non-periodic orbits in a problem of extreme mathematical complexity. In this way, he mathematically evidenced chaotic behavior for the first time. Over time, the chaotic response was evidenced in several systems but still shunned due to its difficulty and unpredictable behavior (OTANI; JONES, 1997).

Modern computers have brought new light to the study of chaos. Numerical calculations from the governing equations became feasible even with their large number of iterations and good precision, thus reaching the solution for several complex and nonlinear systems. Taking advantage of the new computational capacity, Lorentz observed in weather forecasting that a single different digit in the computer's decimal places made his system evolve to completely different responses, noticing the unpredictability in deterministic systems (LORENZ, 1963).

After that, interest in chaos soared, leading to numerous studies where several researchers verified the presence of chaos in the most diverse systems. A new theory verified that the turbulence, in its pressure and velocity variations in a flow, was chaotic (RUELLE; TAKENS, 1971), subsequently verified experimentally (SWINNEY; GOLLUB, 1981). May (1976) notice chaotic behavior in the Logistic Map, a simple nonlinear dynamical equation modeling prey-predator. In chemistry, chaos has been identified experimentally in reactions (OLSEN; DEGN, 1977; ROUX; SIMOYI; SWINNEY, 1983); in mechanical oscillators (MOON; HOLMES, 1979); in electrical circuits (LINSAY, 1981). Mandelbrot studied fractals in several systems, including mathematics, astronomy, chemistry, and biology (MANDELBROT; MANDELBROT, 1982). Later, it was discovered correspondence between the Mandelbrot set and the Logistic map (DEVANEY, 1990).

The discovery of bifurcations was a great advance in the study of chaos, discovered by Feigenbaum (1980). Bifurcations are general behaviors that transition from periodic to chaotic behavior. A series of period doubling in the bifurcation diagrams lead to the chaotic behavior (FEIGENBAUM, 1980).

The next sections present a literature review of chaos control methods.

2.1 Chaos Control

Control systems aim to command, direct, or regulate the behavior of a specific system. Despite having the same objectives, chaos control differs from conventional control techniques in some aspects. The chaos control takes advantage of the great sensitivity to disturbances and the dense set of unstable periodic orbit (UPO) where, with small actions, it stabilizes one of these infinite orbits. These proprieties are not present in non-chaotic responses. Due to the small actuation, this process consumes less energy compared to control techniques not specifically dedicated to chaos control. Furthermore, chaos control has great flexibility; the controller can be designed to make the system transit through different UPOs as needed (OTT; GREBOGI; YORKE, 1990). Moreover, chaos control techniques are based on the geometrical properties of the attractor of the system; therefore, they do not need knowledge of the governing equations of the system.

The first chaos control techniques were developed with the intention of avoiding the chaotic response in the systems. Control methods can be classified as discrete or continuous. The first chaos control method was known as the OGY method, in honor of the authors Ott-Grebogy-York, proposed in Ott, Grebogi & Yorke (1990), which is a discrete method in which the perturbations in a Poincaré section are applied. The first continuous method proposed was the Time-Delayed Feedback (TDF); in this method, the control acts continuously and uninterrupted in the system (PYRAGAS, 1992).

Reviews of discrete methods based in OGY technique are presented in Ditto, Spano & Lindner (1995), Grebogi & Lai (1997), and Boccaletti et al. (2000). A continuous methods review is presented in Pyragas (2006). Furthermore, Savi, Pereira-Pinto & Ferreira (2006) presented a review of chaos control applied to mechanical systems. Paula & Savi (2011) compared various chaos control techniques applied to mechanical systems. The next two subsections introduce these two precursor methods along with some of the methods that enhanced them. Moreover, Schöll & Schuster (2008) presents a handbook summarizing the main chaos control techniques and some applications. Figure 2.1 summarizes this literature review's main chaos control methods.

2.1.1 Discrete methods

In chaotic maps, in the vicinity of fixed points, in general, the interactions have a saddle shape, with a stable direction and an unstable one. The OGY method takes advantage of these properties by imposing small perturbations in order to force the system to fall back on the stable direction, stabilizing the UPO. The Jacobian around the fixed points can derive these acting directions using their eigenvalues and eigenvectors. As the method is discrete, the control action must wait for the system to be in the vicinity of the fixed point to carry out such disturbances. This disturbance aims to force the system in the stable direction to stabilize the desired UPO. The first experimental application of

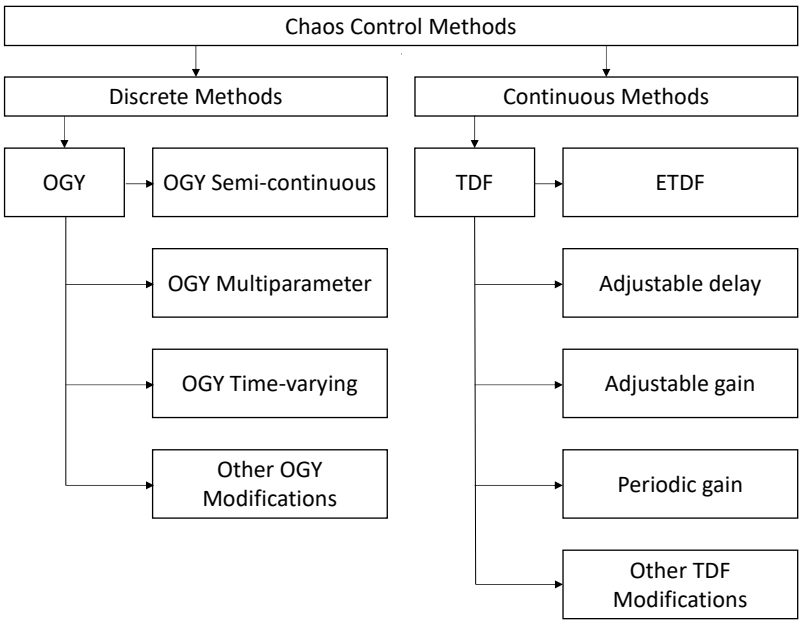

Figure 2.1 – Chaos control methods.

this method was implemented in the control of magnetoelastic ribbon (DITTO; RAUSEO; SPANO, 1990).

Several improvements were presented in subsequent years. Romeiras et al. (1992) expanded the method aiming at n-dimensional systems. This method generalizes OGY, approaching it as a pole allocation, making it more flexible in its gain matrix choice. Gluckman et al. (1997) worked with a high dimensions system with an adaptive control considering a non-stationary system.

Dressler & Nitsche (1992) implemented OGY with a reconstructed attractor using delayed states method. This method modified OGY in a way that the Poincaré section depends on its previous perturbations. So & Ott (1995) extended Romeiras et al. (1992) method with higher dimensions to reconstruct the phase state.

Bayly & Virgin (1994) made considerations about the practical applicability of OGY. This work assessed its implementation of some external factors such as high instability, high nonlinearities, model errors, noise, and uncertainty of the stabilization time. This article led Hübinger et al. (1994) to propose the semi-continuous (SC) OGY method focusing on the high instability problem. In this improvement, control sections are inserted in intermediate phases and equally spaced in the forcing cycle, thus applying the OGY method in each section. Afterward, this idea was applied to systems with reconstructed Poincaré section by delayed coordinates (KORTE; SCHOUTEN; BLEEK, 1995). An extension for this method was proposed to address the control of a high-dimensional double pendulum in Christini, Collins & Linsay (1996). Another distribution for the intermediary sections was proposed in order to equalize the rates of flux expansion between sections (RITZ et al.,

1997).

Another major advance in OGY was the implementation of another control parameter using pole allocation proposed in Barreto & Grebogi (1995). In this method, all parameters can actuate simultaneously in all control sections, thus achieving faster stabilization time and better performance in a noise environment. Paula & Savi (2009b) proposed implementation of a multiparameter approach to OGY and SC-OGY methods. In this modification, it is considered an uncoupled approach, where the passive parameter returns to its original value, and a coupled approach, where each parameter always influences the control.

Christini et al. (1997) proposed a control method without a learning stage; thus, it does not depend on the system's mathematical model; it is in real-time and adaptive. Yu et al. (2001) modified OGY to utilize invariant manifold theory and sliding mode control to avoid the system Jacobian calculation. Alasty & Salarieh (2005) utilized fuzzy estimations in a OGY, making it more robust. Yagasaki (2007) proposed a new method based on OGY in order to stabilize non-periodic trajectories.

2.1.2 Continuous methods

The second main approach to chaos control is the Time-Delayed Feedback (TDF) method proposed by Pyragas (1992). This method applies a continuous perturbation to the system based on feedback on the difference between the current and delayed states of the system. This continuous actuation favors control of highly unstable systems. The discrete actuation of OGY makes it more difficult to stabilize high Lyapunov exponents UPO relative to the inverse of the time elapsed between perturbations (PYRAGAS, 1992). Furthermore, this approach tends to achieve the system's stabilization faster than the discrete techniques. There is a necessity for a steady analysis of the system on methods based on OGY, which does not happen with TDF. TDF method does not depend on the system model; its implementation only depends on the time delay and the control gains. These characteristics make its experimental implementation easier. Pyragas & Tamaševičius (1993) made it the first experimental application to use the control technique in an electronic chaotic oscillator.

Subsequently, this method was applied experimentally in some works. Hikihara & Kawagoshi (1996) use the TDF method to control chaos in a magneto-elastic beam system described by the Duffing equation; Ramesh & Narayanan (2001) use it to control chaos in a two-dimensional airfoil; Galvanetto (2002) stabilizes a system orbit with dry friction; Sugimoto & Osuka (2004) apply it to stabilize a walking bipedal robot; Wei et al. (2004) stabilize an period-1 unstable periodic orbit of a gas discharge plasma. Cai & Chen (2010) implemented experimentally it in flexible structures; Liu, Yan & Wang (2020) was successful in stabilizing chaos in micro and nanoelectromechanical resonators.

The main challenge to the TDF method is the introduction of time-delayed to the system and the control gain choice. Attempting to solve the time-delay problem, Boccaletti & Arecchi (1995), Herrmann (2001) proposed adaptive algorithms to adjust the time-delay. Meanwhile, on the issue of determining the controller's gains, many papers had to choose it by a trial and error method as did Pyragas & Tamaševičius (1993). Pyragas (1992) proposes to evaluate the Lyapunov exponent using the system's motion equation to determine the control gains. Lehnert et al. (2011) proposed adaptive algorithms to adjust the control gains based on the speed gradient method. Several studies implemented a periodic control gain and eliminated some of the problems of the fixed control gain (LEONOV, 2014; PYRAGAS; PYRAGAS, 2016; PYRAGAS; PYRAGAS, 2018). Ding & Lei (2023) introduced a machine learning technique that interacts with the dynamical system to obtain the control gains without the precise mathematical model of the system.

The modification considered most important to the TDF is Extended Time-Delayed Feedback (ETDF) (PYRAGAS, 2006). This method, presented in Socolar, Sukow & Gauthier (1994), uses not only one delayed state of the system but expands it to consider many previous states. Moreover, this implementation introduces a new control parameter related to other delayed states of the system. This implementation attempts to stabilize high periodicity UPOs. Paula & Savi (2009a) used this method to control chaos in a nonlinear pendulum.

Some studies were made in order to verify stability and prove proprieties of TDF and ETDF. Ushio (1996) proved that TDF is able to stabilize only a specific class of UPO characterized by a finite torsion of the state space in discrete systems. Thus, TDF cannot stabilize UPOs with an odd number of Floquet multipliers bigger than one. Thereafter, Just et al. (1997), Nakajima (1997) extended these proprieties to continuous systems, and Nakajima & Ueda (1998b) proved that the same limitation occurs with ETDF. Hooton & Amann (2012) presented a new limitation to TDF and ETDF related to real Floquet multipliers larger than unity.

Several studies have attempted to overcome these limitations. Ushio & Yamamoto (1998) presented modification using nonlinear estimation of stabilised orbits and Ushio & Yamamoto (1999) used predictive algorithm, both for the discrete case. Nakajima & Ueda (1998a) proposed a modification to consider half-period delayed feedback; however, it only worked for symmetric orbits. Pyragas (2001) modified ETDF method to attend to the limitation related to a finite torsion of the state space. This modification added a new unstable variable to the system in order to raise the number of positive Floquet exponents to an even number. This modification was applied experimentally in an electronic system by Höhne et al. (2007).

TDF and ETDF methods were vastly studied; following there are some of their main modifications, improvements and applications. Chen & Yu (1999) presented analytical sufficient conditions for chaos control related to both stabilization and tracking UPO using TDF. Tian et al. (2009) proposed and derived some analytical conditions for a new control

method based on the work of (CHEN; YU, 1999). This method considers different control parameters and successive dislocation of the time-delay feedback.

Vieira & Lichtenberg (1996) generalized ETDF method in order to substitute some portion of the nonlinear dynamical system with delayed dynamics rather than using a linear delay function for control. They also proposed a further generalization in which the control function retains memory of all previous periods. Tian & Yu (2000) adopted optimal control theory to design a TDF controller. The main idea is to minimize a performance index in order to stabilize an UPO.

Aiming to establish a chaotic response, Wang, Chen & Yu (2000) proposed an anti-control chaos method based on the TDF. This method effectively generates chaos or increments it in finite-dimensional, continuous-time, autonomous systems. Wang & Chau (2008) implemented the anti-control chaos experimentally in a permanent magnet DC motor system for vibratory compactors.

Tsai, Fuh & Chang (2002) proposed a method using a sliding mode controller with a time-varying manifold dynamic to control chaos under varying external force and noise conditions. Nazzal & Natsheh (2007) presented a controller based on the nonlinear sliding mode and applies it to Chua's circuit and Lorenz system. Based on the same theory, Bessa, Paula & Savi (2009) introduced an adaptive fuzzy sliding mode controller to address the model uncertainties. The convergence proprieties were proven analytically, and the method was applied numerically to a nonlinear pendulum.

3 Nonlinear Dynamics and Chaos

This chapter presents some topics in nonlinear dynamics concerning chaotic responses, analysis tools, and control strategies.

The tools applied to the study of the dynamics of nonlinear systems can be divided into two categories. The first is the qualitative approach that aims to understand the global behavior of the system as well as its dynamic evolution. The second is the quantitative approach that explores the temporal evolution of the system (SAVI, 2006).

The qualitative study uses topology-based geometric techniques, with the Poincaré map and the bifurcation diagram as its main concepts. These concepts are also necessary for the quantitative approach, as they provide a global understanding of system behavior. The quantitative study addresses the determination of dynamic invariant parameters, such as the Lyapunov exponent.

This chapter also introduces the close return method, based on recurrent points (AUERBACH et al., 1987a), used to identify the unstable periodic orbits immersed in the system's chaotic attractor. Finally, the chapter briefly presents the main chaos control methods and addresses the continuous chaos control technique Extended Time-Delayed Feedback method.

3.1 Poincaré Map and Poincaré Section

The Poincaré map is a substate of the phase space that allows the analysis of a continuous dynamic system in time (flow) in a discrete system (map), creating a secondary system with a lower dimension. The transformation aims to capture a set of positions in phase space.

For its construction, it must be intersecting the trajectory with a hyperplane. The plane is arbitrarily chosen in phase space and must be perpendicular to the trajectory. Thus, the set of system points is called the Poincaré map, and the chosen hyperplane is called the Poincaré section (OTANI; JONES, 1997). Figure 3.1 represents the construction of the section in different forcing phases. In this way, the dimension of the system is reduced, excluding time, since the trajectory sample is made in a discrete time interval.

Although there is no general methodology for constructing a Poincaré section.

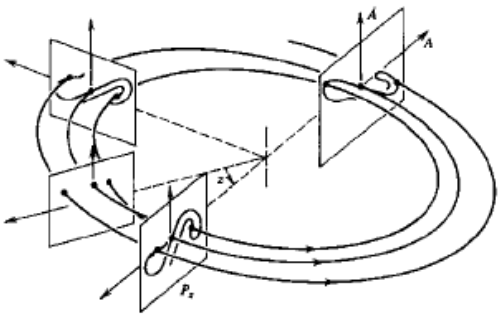

Figure 3.1 – Construction of the Poincaré map (MOON, 1992).

Usually, the section is related to a specific forcing phase in systems subjected to periodic forcing. Thus, the sample period is given by $T/nm = 2\pi/\omega$, where ω is the excitation frequency, and nm defines the time step, dividing the forcing period into nm points. Algorithm 3.1 presents this work implementation. In this algorithm, np corresponds to the total integration time, equivalent to np forcing pe.

Algorithm 3.1 Poincaré map

```
/*Loop for total time evolution */
for jp = 1; jp ≤ np; jp++ do
    /*Loop for one forcing period evolution */
    for jn = 1; jn ≤ nm; jn++ do
        x() ← f(x());
        /*Poincaré map */
        if jn == 1 then
            poincare(jp) ← x(i)
        end
    end
end
```

The Poincaré map indicates the type of the behavior. For periodic regimes, the Poincaré map presents a finite number of points. If the periodicity of the orbit is multiple of the forcing frequency (considering a harmonically excited system), the map presents the same number of points as the periodicity of the response. Figure 3.2a illustrates both periodic and chaotic responses obtained numerically. Magenta dots represent the Poincaré maps, while the black line is the phase space. In a quasi-periodic regime, the Poincaré map presents a closed curve. Finally, in a chaotic regime, the Poincaré map presents an infinite set of points, generally with fractal geometry distributed in a lamellar structure, with empty and dense regions. If the system's response is chaotic, the maps is related to a chaotic attractor, while if it presents transient chaos, it is associated with a chaotic saddle.

An attractor is a topological invariant set of the system to which the orbits of the system tend to converge. A chaotic attractor visualization in a Poincaré map shows a collection of points arranged in an organized manner.

In non-dissipative chaotic regimes, a cloud of points tends to fill the space. However, systems in chaotic dissipative regimes are characterized by the horseshoe transformation,

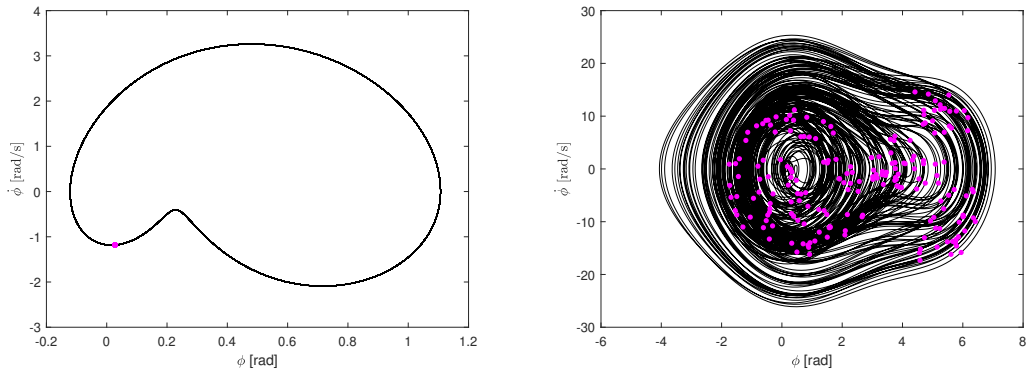

(a) Period-1; (b) Chaotic;

Figure 3.2 – Poincaré section:
Poincaré section: ·
Orbit: —

characteristic of the Cantor set. Attractors can be said to be chaotic or strange, and maybe both or just one of them simultaneously (GREBOGI et al., 1984).

The strange attractor is a geometric feature of the system, where it represents the preferential region of the phase space that attracts the states of the system and has a fractal structure of the Cantor set type (SAVI, 2006). The chaotic attractor, however, is a physical feature that the Poincaré map visualizes as a collection of points arranged in an organized way. The chaotic attractor is ergodic, meaning that each point of this set is visited during the system's evolution (PEREIRA-PINTO; FERREIRA; SAVI, 2004).

Unlike the attractor, the chaotic saddle in chaos has a repulsive characteristic and is present in the case of transient chaos. It also has a finite number of points in the Poincaré section. Chaotic saddles also have a fractal nature, just like the strange attractor.

3.2 Bifurcation Diagram

A bifurcation diagram presents the system's response influence to a variation of one of its parameters. This provides a global visualization and allows us to evaluate where and how the changes in the system response occur. Usually, a small change in a parameter results in a small quantitative change. However, a bifurcation occurs when a small parameter change results in a qualitative change.

One can differentiate bifurcations into local bifurcations and global bifurcations. Local bifurcations deal with a limited region of phase space and deal with, for example, period doubling. A system can present multiple local bifurcations while it does not have a qualitative change in the response, so it does not show chaotic behavior. Global bifurcations, however, characterize a sudden change in the topology and structure in the phase space, which are not restricted locally. Global bifurcations are present in the transition from periodic to chaotic behavior or collisions.

There is no single way to draw a bifurcation diagram. For this work, the brute force method was adopted (PARKER; CHUA, 2012). This method simulates different values of the parameter to be evaluated, varying it quasi-statically while analyzing some responses in the Poincaré section. Algorithm 3.2 presents a pseudo-code for this method, where α is the parameter that is varied, α_0 is its initial condition, $d\alpha$ is the step, x_0 is the initial conditions for each α.

Algorithm 3.2 Brute force bifurcation diagram

```
/*Parameter quasi-static varying */
for α = α_0; α ≤ α_max; α = α + dα do
    x ← x_0
    interval = nm/ns
    /*Loop for time evolution */
    for jp = 1; jp ≤ np; jp++ do
        /*Loop for cycle evolution */
        for jn = 1; jn ≤ nm; jn++ do
            x() ← f(x());
            /*Poincaré sections */
            if jn == 1 then
                poincare(N) ← x(i)
            end
            i ← i + 1
        end
    end
end
```

Figure 3.3 shows the bifurcation diagram for the limit set of the Logistics Map when varying the growth rate of a population. The Logistics Map is a polynomial mapping given by $x_{n+1} = rx_n(1 - x_n)$, where $0 \leq x_n \leq 1$ represents a ratio of existing population to the maximum possible population and r represents the growth rate. The growth rate is varied to construct the bifurcation diagram. It is possible to observe both local bifurcations, where the period doubles, and global bifurcations, where the system changes from periodic to chaotic behavior.

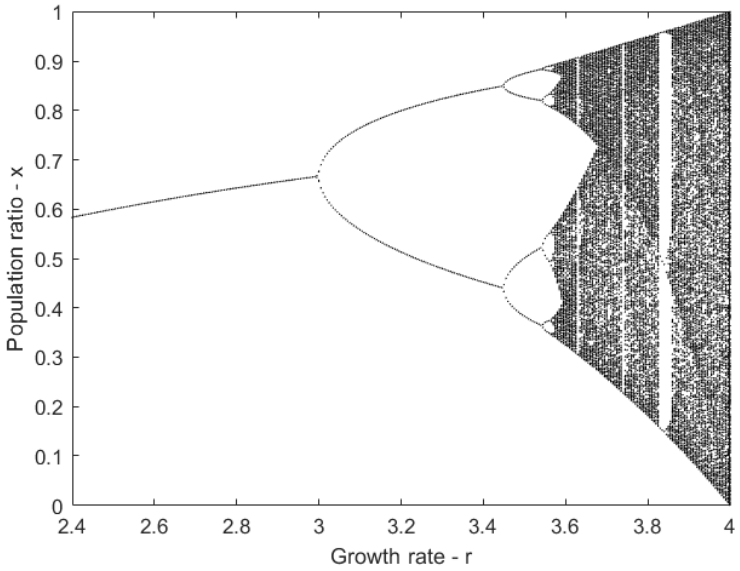

Figure 3.3 – Bifurcation Diagram of Logistic Map.

3.3 Unstable Periodic Orbits Identification

In general, the initial phase of the control methods is the learning stage, where we need to identify unstable periodic orbit (UPO) and to determine controller gains. The second phase consists of the control itself and will be discussed further in the text.

Systems in chaotic regimes are characterized by an infinity of unstable periodic orbits combined with great sensitivity to initial conditions and their ergodic characteristic. The existence of these infinite periodic patterns makes chaotic systems very flexible (ECKMANN; RUELLE, 1985). The ergodic character of the system indicates that all points close enough to the attractor are visited by the chaotic trajectories at some point in their evolution (AUERBACH et al., 1987a).

The UPOs are periodic patterns within a system attractor that are part of the set of topological invariants of the system and, thus, do not suffer topological change with the change of coordinates (GUNARATNE; LINSAY; VINSON, 1989). Other topological invariants of the system can be determined from the UPOs such as the Lyapunov exponent and the fractal dimension of the system (AUERBACH et al., 1987a).

The identification of UPOs can be made by temporal analysis or by the explicit equation of motion (XU et al., 2002). There are several algorithms for its determination depending on the specific characteristics of each series. In order to identify UPOs, this work uses the close-return method (AUERBACH et al., 1987a).

Close-return method is implemented on a Poincaré section in such a way that a scan of the entire time series is performed, looking for pairs of points that satisfy the

condition:

$$|\xi_i - \xi_{i+k}|_{i=1}^{(N-k)} \leq r_1 \tag{3.1}$$

where N is the total number of points in the Poincaré section, r_1 is the tolerance with which recurrent points are distinguished, and k is the maximum period of the orbit to be found. In this way, we store the points $\{\xi_i, \xi_{i+1}, \ldots, \xi_{i+k-1}\}$ that satisfy the condition and belong to the k- orbit periodic in the control Poincaré section. During the search, a given orbit can be visited more than once, so verifying identical orbits within a r_2 tolerance and with a permutation of their points is necessary. In the case of equivalent orbits, for the same period, the real orbit is approximated by the arithmetic mean (SAVI, 2006).

3.4 Lyapunov Exponent

The Lyapunov exponents are a geometric invariant of the system response and are widely used to characterize chaos. Unlike the tools presented above, the Lyapunov exponent is a quantitative measure of the system and can, therefore, formally characterize it. The exponent evaluates the predictability of system response and can be used to evaluate the capability of an UPO to be stabilized.

The methods to evaluate the Lyapunov exponent of a temporal series can be classified into trajectory and perturbations methods. The idea behind the trajectory methods is to relate the evolution of the distance of two close trajectories. Conversely, the perturbations methods are based on the Jacobian matrix estimation of the trajectory, which is used to evaluate the Lyapunov spectrum. This work uses the trajectory method proposed by Wolf et al. (1985).

To evaluate the Lyapunov exponents, we consider a reference path $\Phi(x_1, t)$ and define a neighborhood hypersphere with diameter d_0 at the initial instant t_0. In the neighborhood, a second trajectory $\Phi(x_2, t)$ is defined in which x_2 is contained in the previously defined hypersphere. The set of Lyapunov exponents that generates the dimension of the hypersphere is associated with the dimension of the dynamical system. With its temporal evolution, evaluate the divergence or convergence of the second trajectory in relation to the first. Figure 3.4 geometrically represents the time evolution in which the deformation of the hypersphere into a hyperellipsoid occurs.

Thus, the diameter of the hypersphere can be expressed by:

$$d(t) = d_0 b^{\lambda t} \tag{3.2}$$

where b is a base of reference for the logarithm. Thus, the Lyapunov exponent is defined as:

$$\lambda = \frac{1}{t} \log_b \left(\frac{d(t)}{d_0} \right) \tag{3.3}$$

Thus, the sign of the Lyapunov exponent defines the divergence as positive and the convergence as negative. The stability of a trajectory is associated with the negative

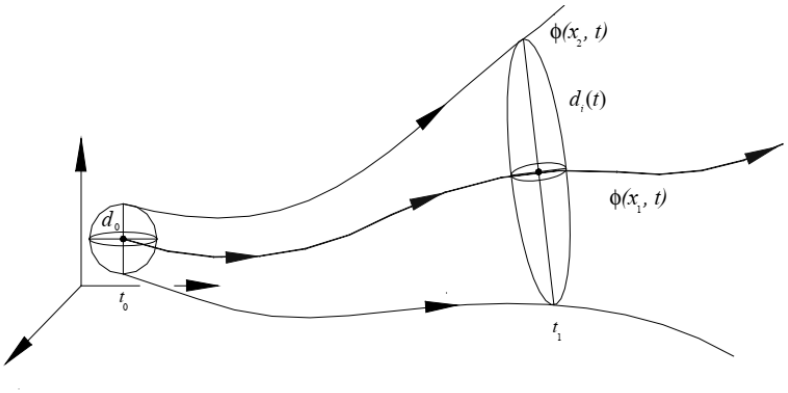

Figure 3.4 – Lyapunov exponent (SAVI, 2006).

sign of the exponent, while the instability is associated with the positive sign. It is worth noting that each degree of freedom of the system is associated with a different exponent. Thus, a system with at least one positive exponent is associated with a local divergence that characterizes the typical sensitivity to initial conditions of chaos. Therefore, for a non-autonomous system, it is enough to evaluate the greatest Lyapunov exponent to analyze the stability of an UPO (PYRAGAS, 1995).

When a reference trajectory is evaluated, it will diverge from the evaluated trajectory if it is chaotic. However, the Lyapunov exponent can only be calculated in the vicinity of the reference path where the linearization is valid. To define the Lyapunov exponent by the dynamical system extension and monitor the neighboring trajectories, Wolf et al. (1985) proposed an evaluation of the average of the exponential growth in several trajectory points. To this end, every time the distance $d(t)$ becomes too large, a new $d_0(t)$ is defined in which the divergence is reassessed, as shown in Figure 3.5. The distance d_0 is defined as the Euclidean norm between the points in the neighborhood Q_0 and in the system P_0. Then, the evolution of these 2 points is evaluated up to a time t_1, two new points P_1 and Q'_1 are defined, and a new tangential distance $d(t_1)$. That is, each time the exponent moves away from the reference trajectory, a value of the exponent is taken, and a new evaluation begins in the neighborhood of the system.

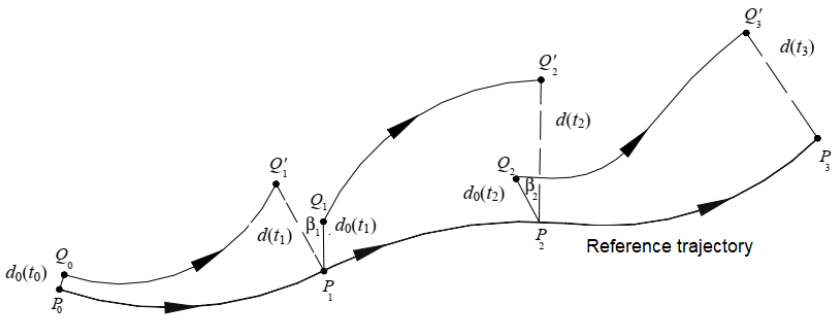

Figure 3.5 – Calculation of the Lyapunov exponent (SAVI, 2006).

Thus, for this type of evaluation, the Lyapunov exponent is defined as:

$$\lambda = \frac{1}{t_n - t_0} \sum_{k=1}^{n} \log_b \left(\frac{d(t_k)}{d_0(t_{k-1})} \right) \tag{3.4}$$

3.5 Chaos Control

Chaos control exploits the unique characteristics of systems that exhibit chaotic responses. Thus, it consists of applying small perturbations to the system to stabilize it in a specific unstable periodic orbit. This allows the dynamic system to move from orbit to orbit according to need, giving it great flexibility.

The Time-Delayed Feedback (TDF) method proposed in Pyragas (1992) was the first continuous method proposed in the literature, acting continuously and uninterrupted in the system. Continuous methods favor the control of systems that have high Lyapunov exponents. Continuous controllers are also less sensitive to external noise than discrete controllers (PAULA; SAVI, 2011). ETDF improves on TDF in terms of stabilizing time and robustness. This work investigates a generalized form of the ETDF.

3.5.1 Extended Time-Delayed Feedback Method (ETDF)

The ETDF method is applied to dynamical systems modeled by systems of nonlinear ordinary differential equations of the form:

$$\dot{\mathbf{x}}(t) = \mathbf{f}(\mathbf{x}, t) + \mathbf{B}(t) \tag{3.5}$$

where $\mathbf{x}(t) \in R^n$ is the vector containing the state variables, $\mathbf{f}(\mathbf{x}, t) \in R^n$ defines the dynamics of the system and $\mathbf{B}(t) \in R^n$ is associated with the control.

Therefore, the control law is given by:

$$\mathbf{B}(t) = \mathbf{K}[(1 - R)S_\tau - x] \tag{3.6}$$

with,

$$\mathbf{S}_\tau = \sum_{m=1}^{\infty} R^{m-1} \mathbf{x}_{m\tau} \tag{3.7}$$

where $\mathbf{K} \in R^{n \times n}$ is the gain matrix, τ is the time delay, $0 \leq R < 1$ is a controller parameter related to delayed states, $x = x(t)$ and $\mathbf{x}_{m\tau} = \mathbf{x}(t - m\tau)$, and m represents the number of the delayed state. Usually, the literature uses the $\mathbf{K}$ as a scalar K.

While the TDF considers only one delayed state of the system in the control law, the ETDF considers several. Notably, for $R = 0$, the equation falls under the control law of the TDF method, where only a single delayed state of the system is considered.

When the system trajectory is correspond to an UPO, the Equation (3.6) is null for any R since $\mathbf{x}(t - m\tau) = \mathbf{x}(t)$ for all m and $\tau = T_i$, where T_i is the periodicity of the ith UPO.

In this work, it is considered 3 delayed states, $m = 3$. Thus,

$$\mathbf{S}_\tau = \mathbf{x}(t-\tau) + R\mathbf{x}(t-2\tau) + R^2\mathbf{x}(t-2\tau) \tag{3.8}$$

Differential equations govern the dynamical system with the controller with time delay Delayed Differential Equation (DDE). Unlike ODEs that have their solution system's current state of the system, the solution of DDEs dependencies on previous states.

The term S_τ has information for $t < m\tau$; therefore, the evaluation of the DDE has to wait for the system evolution. This work's control action starts when all delayed states are known. This way, for the adopted value $m = 3$, the control starts when $t > 3\tau$.

The learning stage in continuous methods consists of identifying the UPO that you want to stabilize and determining the gain $\mathbf{K}$ and if using ETDF, the gain R. The control phase starts with the defined gains, and its gains are used to determine the necessary disturbances.

The ETDF control method occurs continuously in the system (KITTEL; PYRAGAS; RICHTER, 1994). This control acts by slightly modifying the Lyapunov exponent in the UPO of interest, making it stable. For this, the control gains must be chosen in such a way that all Lyapunov exponents become negative (KITTEL; PARISI; PYRAGAS, 1995).

However, it is sufficient to determine the largest Lyapunov exponent in a non-autonomous system to stabilize the UPO (PYRAGAS, 1995). Thus, for a constant value of R, an interval of values for K can be determined. That is, to achieve stabilization of a given UPO, the controller gains must be defined so that the largest Lyapunov exponent is less than zero, $\lambda(K, R) < 0$. It is also proposed to adopt gains associated with minimum values of $\lambda(K, R)$ so that there is a greater convergence in close orbits, making it less susceptible to noise.

For the ETDF method with 3 states delayed in time, we have the following DDE:

$$\dot{\mathbf{x}} = \mathbf{f}(\mathbf{x}, t) + \mathbf{B}(t, \mathbf{x}, \mathbf{x}_\tau, \mathbf{x}_{2\tau}, \mathbf{x}_{3\tau}) \tag{3.9}$$

Therefore, to calculate $\mathbf{x} = \mathbf{x}(t)$ in a time greater than t, the function $\mathbf{x}(t)$ must be known in the interval $(t - 3\tau, t)$. The Equation (3.9) has an infinite dimension system and, consequently, infinite Lyapunov exponents. Numerically, it is only possible to determine a finite number of exponents, but it is enough to determine the largest exponent to verify (VICENTE et al., 2005) stability.

3.5.2 Determining gains from the Lyapunov exponent

The choice of suitable gains R and K makes the stabilization of the system in a specific UPO to be achieved. Such values are determined during the system learning phase.

To calculate the Lyapunov exponent, the continuous evolution of the infinite-dimensional system is approximated by a finite number of elements whose values change in discrete steps over time (FARMER, 1982). With this, the function $x_i(t)$, with $i = 1, \ldots, n$, in the interval $(t-3\tau, t)$ can be approximated by N spacing samples $\Delta t = 3\tau/(N-1)$. The system goes from n state variables to $n(N+1)$ variables. A vector z is used to represent these state variables, where $z_{n+1}, \ldots, z_{n(N+1)}$ are related to the states delayed in time of $x(t)$ in the form:

$$(z_1, z_2, \ldots, z_n, \ldots, z_{n+N}, \ldots, z_{n+(n-1)N+1}, \ldots, z_{n(N+1)}) = (x_1(t), x_2(t), \ldots, x_n(t), \\ x_1(t-\Delta t), \ldots, x_1(t-N\Delta t), \ldots, x_n(t-\Delta t), \ldots, x_n(t-N\Delta t)) \quad (3.10)$$

In this work, the approach presented in Sprott (2007) is used, where the DDE is replaced by a set of ODEs. Therefore, the infinite-dimensional continuous system is represented by a system of $n(N+1)$ finite-dimensional ODEs, allowing its resolution by any method indicated for nonlinear ODEs. Like this:

$$\begin{cases} \dot{z}_j = Q_j(z_1, z_2, \ldots, z_n) + B_j(t, z_1, \ldots, z_n, z_{n+1}, \ldots, z_{n(N+1)}) & \text{for } 1 \leq j \leq n \\ \dot{z}_{n+1+(j-1)N} = N(z_j - z_{n+2+(j-1)N})/2\tau & \text{to } 1 \leq j \leq n \\ \dot{z}_{n+i+(j-1)N} = N(z_{n+i+(j-1)N-1} - z_{n+i+(j-1)N+1})/2\tau & \text{for } 2 \leq i \leq (N-1) \\ & \text{e } 1 \leq j \leq n \\ \dot{z}_{n+jN} = N(z_{n+jN-1} - z_{n+jN})/\tau & \text{for } 1 \leq j \leq n \end{cases} \quad (3.11)$$

where $N = 3\tau/\Delta t + 1$. The calculation of the Lyapunov exponent can be performed from these equations by the (WOLF et al., 1985) algorithm. It is also possible to calculate the exponent of an UPO of interest by integrating the system along its orbit. With this, it is possible to choose the control gains adopted to stabilize the UPO.

With this, including the equations of motion in Eq. (3.11) and their linearizations, one obtains a set of $(N+2)^2 + (N+2)$ ODEs that allow the implementation of the algorithm of (WOLF et al., 1985), which evaluates the UPO time series. The system can be reduced to just $N+2$ variables to calculate only the largest Lyapunov exponent with a modification to the algorithm. Due to the large number of ODEs to be solved, the learning phase has a high computational cost.

The algorithm checks the greatest Lyapunov exponent for specific controller gains. To evaluate the stabilization capacity of an UPO, the exponent must be calculated for several gains of the controller. Thus, the choice of controller gains related to negative exponent values can, by hypothesis, stabilize the chosen orbit. Furthermore, the minimum value of the exponent provides a higher rate of convergence of close orbits and makes the method more robust to (PYRAGAS, 1995) noise.

4 Nonlinear Pendulum

This chapter presents the nonlinear pendulum studied in this work. This system has been previously studied by different authors (BLACKBURN; BAKER, 1998; FRANCA; SAVI, 2001), (PINTO; SAVI, 2003), (PAULA; SAVI; PEREIRA-PINTO, 2006), (PAULA, 2010). Initially, the mathematical model is obtained without and with control action considering the generalized ETDF method. In the sequence, the dynamical response without control is evaluated, showing a general overview of system behavior.

4.1 Mathematical Model

Consider the mechanical pendulum shown in Figure 4.1. The apparatus consists of a metallic disk (1) with an eccentrically concentrated mass (3). The disk is fixed to the axis of a rotation sensor (4) and a magnetic device (2) that allows adjusting the energy dissipation of the system, acting as damping. The wires with springs (8) act as an elastic element of the system, providing torsional rigidity. One of the ends of the wire is connected to an electric motor (6) that supplies energy to the system, exciting the pendulum through a pulley connected to the axis of the rotation sensor. The motor is powered by a power source (5), which regulates the rotation frequency by varying the electrical output voltage.

The simplified representation presented in Figure 4.2 is considered for mathematical modeling in which the forces acting on the disk axis and dimensional aspects of the apparatus, used to describe the dynamics of the system, are represented.

Initially, it is considered the balance of moments about the axis of rotation of the disc. The angular position, ϕ, is considered to be zero at the lowest point of its path, and a positive for counterclockwise rotation is assumed. It is also assumed that the forcing phase, θ_{force}, is null when the rod is at the highest point of its trajectory, also assumed positive in the counterclockwise direction.

From the free-body diagram, presented Figure 4.2(b), and the geometric configurations, shown in 4.2(c), we have the external forces exerted by the wire-spring sets F_1 and F_2 are given by the following equations:

$$F_1 = k\left(\sqrt{a^2 + b^2 - 2ab\cos(\bar{\omega}t)} - (a-b) - \frac{d}{2}\phi\right) \tag{4.1}$$

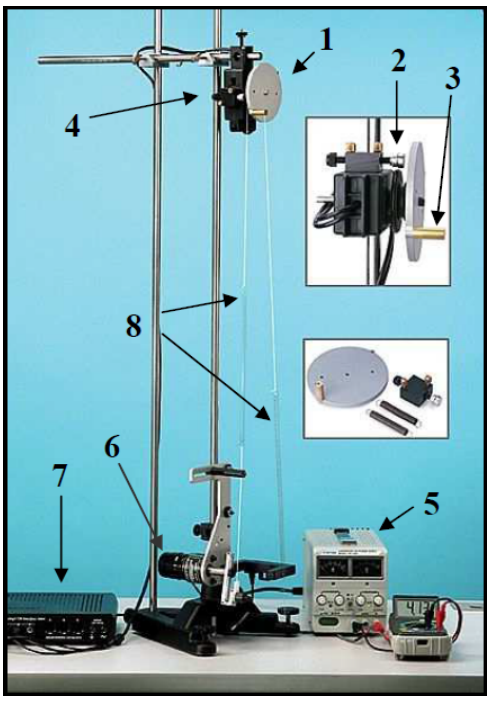

Figure 4.1 – Nonlinear pendulum and accessories: (1) Metal disk, (2) Damping device, (3) Eccentric mass, (4) Rotation sensor, (5) Power source, (6) electric motor, (7) data acquisition device, and (8) springs and wires (PAULA; SAVI; PEREIRA-PINTO, 2006).

$$F_2 = \frac{kd}{2}\phi \tag{4.2}$$

where a is the distance from the electric motor shaft to the wire guide, b is the length of the electric motor rod, d is the diameter of the driving pulley of the metal disc, k is the spring stiffness constant, and $\bar{\omega}$ is the rotation frequency of the forcing electric motor.

The sum of moments arising from the wire-spring sets, weight, and viscous damping and dry friction is given by:

$$\sum \mathrm{T} = \frac{F_1 + F_2}{2}d - \mu\,\mathrm{sgn}(\dot{\phi}) - \zeta\dot{\phi} - \frac{mg\sin(\phi)}{2}D = I\ddot{\phi} \tag{4.3}$$

where m is the concentrated mass value, ζ represents the viscous damping constant, μ represents the dry friction constant, sgn is the sign function, D is twice the distance of the concentrated mass to the axis of the rotation sensor, g is the acceleration of gravity, and I is the moment of inertia of the disc and mass set.

Substituting the Equations (4.1) and (4.2) into Equation (4.3) we obtain the equation of motion:

$$\ddot{\phi} + \frac{\zeta}{I}\dot{\phi} + \frac{kd^2}{2I}\phi + \frac{\mu\,\mathrm{sgn}(\dot{\phi})}{I} + \frac{mgD\sin(\phi)}{2I} = \frac{kd}{2I}\left(\sqrt{a^2 + b^2 - 2ab\cos(\ bar\omega t)} - (a-b)\right) \tag{4.4}$$

The equation exhibits a discontinuity due to the term representing dry friction. The discontinuity comes from the fact that the friction has the same module but with a positive or negative sign depending on the direction of the velocity. This sign change

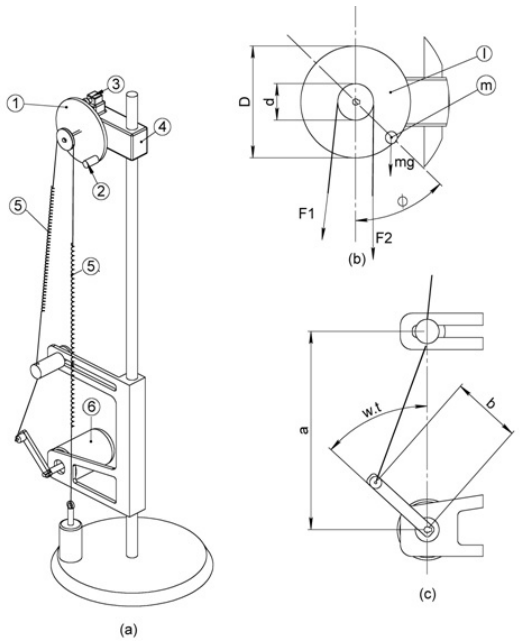

Figure 4.2 – Nonlinear pendulum representation: (a) Physical model: 1-Metallic disk, 2-Eccentric mass, 3-Damping device, 4-Rotation sensor, 5-Wire-spring set and 6-Electric engine; (b) Metal disc: geometry and acting forces; and (c) Excitation system: geometry (PAULA; SAVI; PEREIRA-PINTO, 2006).

characteristic is instantaneous; therefore, it entails a non-smooth discontinuous function that can generate numerical errors that tend to propagate. To avoid this problem, we can apply the following function to smooth out the term (LEINE, 2000):

$$\mu \operatorname{sgn}(\dot{\phi}) = \frac{2}{\pi}\mu \arctan(q \cdot \dot{\phi}) \tag{4.5}$$

where q takes on a large value as $q = 10^6$.

Substituting the Equation (4.5) into (4.6) and rewriting the equation of motion in the form of a system of first-order ordinary differential equations as a function of the state variables $(x_1, x_2) = (\phi, \dot{\phi})$, one obtains:

$$\begin{Bmatrix} \dot{x_1} \\ \dot{x_2} \end{Bmatrix} = \begin{bmatrix} 0 & 1 \\ -\frac{kd^2}{2I} & -\frac{\zeta}{I} \end{bmatrix} \begin{Bmatrix} x_1 \\ x_2 \end{Bmatrix} + \begin{Bmatrix} 0 \\ \frac{kd}{2I}\Delta(t) - \frac{mgD}{2I}\sin(x_1) - \frac{2\mu}{I\pi}\arctan(q\ x_2) \end{Bmatrix} \tag{4.6}$$

where $\Delta(t) = (\sqrt{a^2 + b^2 - 2ab\cos(\bar{\omega}t)} - (a - b)$.

It is assumed the same parameters presented for all numerical simulations: $a = 1.6 \times 10^{-1}$ m; $b = 6.0 \times 10^{-2}$ m; $d = 4.8 \times 10^{-2}$ m; $D = 9.5 \times 10^{-2}$ m; $m = 1.47 \times 10^{-2}$ kg; $I = 1.738 \times 10^{-4}$ kg m^2; $k = 2.47$ N/m; $\zeta = 2.368 \times 10^{-5}$ kg m^2 s^{-1}; $mu = 1.272 \times 10^{-4}$ Nm; $\omega = 5.61$ rad/s (PAULA; SAVI; PEREIRA-PINTO, 2006).

4.2 Mathematical Model with Generalized ETDF Control

Chaos control in the nonlinear pendulum involves introducing small perturbations to the system. These perturbations are applied through actuators that are connected to

the pendulum, introducing small torques.

The actuation of the control parameter, Δl, consists of a variation of the length of the wire-spring set at the end that is not connected to the electric motor, as illustrated in Figure 4.3.

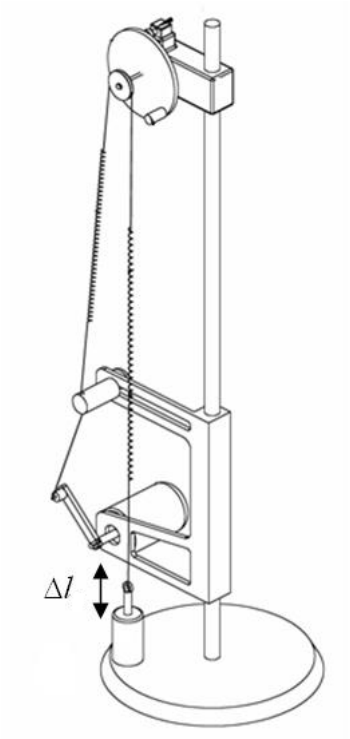

Figure 4.3 – Control actuation schematic representation (PAULA, 2005).

Rewriting the Equation (4.6) in the form of a system of first-order ordinary differential equations as a function of the state variables $(x_1, x_2) = (\phi, \dot{\phi})$ and introducing the controller action $\mathbf{B}(t)$:

$$\begin{Bmatrix} \dot{x_1} \\ \dot{x_2} \end{Bmatrix} = \begin{bmatrix} 0 & 1 \\ -\frac{kd^2}{2I} & -\frac{\zeta}{I} \end{bmatrix} \begin{Bmatrix} x_1 \\ x_2 \end{Bmatrix} + \begin{Bmatrix} B_1(t) \\ \frac{kd}{2I}\Delta f(t) - \frac{mgD}{2I}\sin(x_1) - \frac{2\mu}{I\pi}\arctan(qx_2) + B_2(t) \end{Bmatrix} \tag{4.7}$$

where:

$$\mathbf{B}(t) = \begin{Bmatrix} B_1(t) \\ B_2(t) \end{Bmatrix} = \begin{bmatrix} k_{11} & k_{12} \\ k_{21} & k_{22} \end{bmatrix} \begin{Bmatrix} (1-R)S_{\tau 1} - x_1 \\ (1-R)S_{\tau 2} - x_2 \end{Bmatrix} \tag{4.8}$$

Usually, the literature presents the formulation where only the term k_{22} is non-null, representing a torque that is exclusively dependent on the pendulum velocity. In this context, the gain matrix $\mathbf{K}$ is reduced to a scalar, denoted as follows:

$$\mathbf{K} = \begin{bmatrix} K_{11} & K_{12} \\ K_{21} & K_{22} \end{bmatrix} = \begin{bmatrix} 0 & 0 \\ 0 & K_{22} \end{bmatrix} = \begin{bmatrix} 0 & 0 \\ 0 & K \end{bmatrix} \tag{4.9}$$

With this assumption, $B_1 = 0$ and $B_2 = -\frac{kd}{2I}\Delta l(t)$. Thus, from Eq. 4.8 the value of $\Delta l(t)$ is given by:

$$\Delta l = -\frac{2I}{kd}K[(1-R)S_{\tau 2} - x_2] \tag{4.10}$$

This work explores all terms of the gain matrix $\mathbf{K}$. Thus, from Equation 4.8 we obtain:

$$\begin{Bmatrix} B_1(t) \\ B_2(t) \end{Bmatrix} = \begin{Bmatrix} K_{11}[(1-R)S_{\tau 1} - x_1] + K_{12}[(1-R)S_{\tau 2} - x_2] \\ K_{21}[(1-R)S_{\tau 1} - x_1] + K_{22}[(1-R)S_{\tau 2} - x_2] \end{Bmatrix} \tag{4.11}$$

The control action $B_1(t)$ is associated with imposing a change in angular velocity on the system. On the other hand, the control action for $B_2(t)$ is associated with a torque, which is related to the variation of the length of the wire-spring set illustrated in Figure 4.3, and is given by:

$$B_2 = -\frac{kd}{2I}\Delta l = K_{21}[(1-R)S_{1\tau} - x_1] + K_{22}[(1-R)S_{2\tau} - x_2] \tag{4.12}$$

where $S_{i\tau} = x_i(t-\tau) + Rx_i(t-\tau) + R^2x_i(t-\tau)$ with $i = 1, 2$.

4.3 Dynamical Response without Control

The nonlinear pendulum subjected to periodic forcing can exhibit various responses. A bifurcation diagram is constructed to conduct a comprehensive analysis of the potential system behaviors. The system response is acquired through numerical integration of the mathematical model, employing a fourth-order Runge-Kutta method. In all computations, a time step of $h = \frac{2\pi}{150\bar{\omega}}$ was used. The bifurcation diagram depicts the angular position for a frequency excitation ranging from 3.0 rad/s to 7.0 rad/s with increments of 0.004 rad/s. The initial conditions are null for the first forcing cycle. For each forcing frequency, a time integration of 200 forcing cycles was performed, with the initial 50 periods being disregarded as transient. The bifurcation diagram is shown in Figure 4.4.

From the bifurcation diagram, one can notice distinct regions related to periodic and a non-periodic motions. For lower frequencies, in the range of $3.00 \leq \omega \leq 5.32$ rad/s we observe a periodic motion of periodicity one. This periodic region is followed by a chaotic region from $5.33 \leq \omega \leq 5.78$ rad/s and $5.87 \leq \omega \leq 5.91$ rad/s. In the range $5.78 \leq \omega \leq 5.87$ we observe a periodic window. For frequencies higher than $\omega = 6.096$, we observe periodic motion region.

For the chaotic behavior analysis, the forcing frequency $\omega = 5.61$ rad/s was chosen, which is within the chaotic region identified by the bifurcation diagram. Figure 4.5 shows the Poincaré map for the chosen forcing frequency, considering two different Poincaré

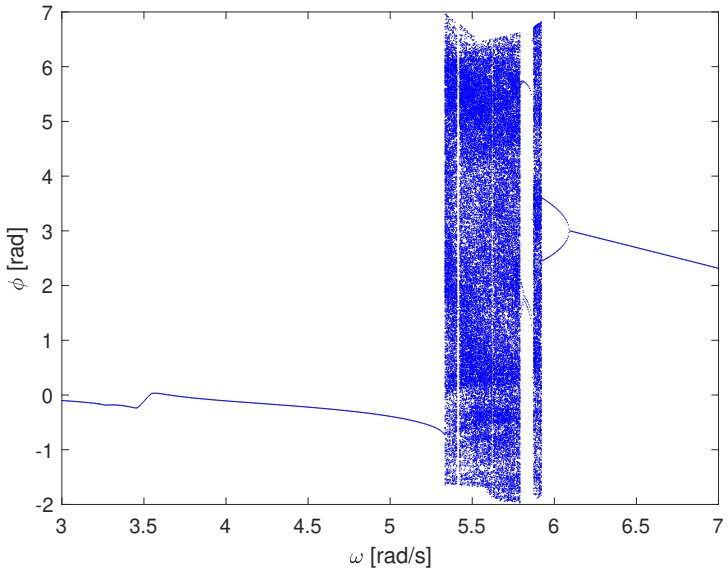

Figure 4.4 – Bifurcation Diagram.

sections. These sections are defined with respect to the forcing phase, with one located at 0 rad and the other at π rad. The control method is applied to this chaotic behavior.

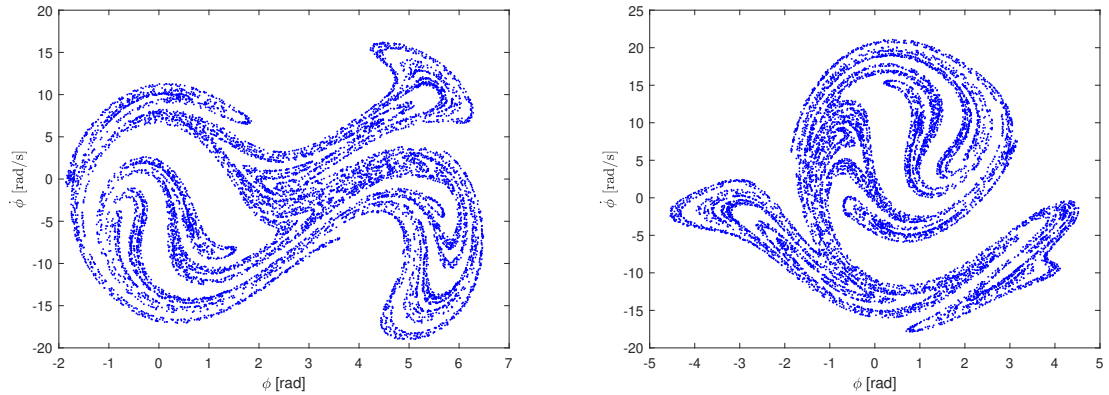

(a) Forcing phase: 0 rad.

(b) Forcing phase: π rad.

Figure 4.5 – Poincaré Sections for $\omega = 5.61$ rad/s.

5 Learning Stage

This chapter presents the first step of chaos control strategy: the learning stage. The learning stage consists of identifying the UPOs and determining the control gains. In the present work, the gains were chosen from the maximum Lyapunov exponent of each UPO.

5.1 Unstable Periodic Orbits Identification

The learning stage's initial phase involves identifying the UPOs targeted for stabilization. To achieve this objective, the simulation used an integration time of 20000 forcing cycles, where the initial 150 forcing cycles were discarded as transient. The initial conditions considered were null.

The identification of UPOs was accomplished through the close-return method (AUERBACH et al., 1987b) with a tolerance of $r_1 = 0.01$. This method relies on recurrence points in the Poincaré map. From the generated time series, considering the adopted tolerance and periodicity up to 6, 15 unstable periodic orbits were identified. Table 1 shows the number of UPOs identified for each periodicity.

Orbits with periodicities 1, 2 and 3 were selected for stabilization. In Figure 5.1a the chaotic attractor is presented together with the chosen UPOs. Additionally Figures 5.1(b-d) depict UPOs of period-1, period-2 and period-3, respectively, in phase space.Table 2 provides the Lyapunov exponent for each selected UPO without control, showing their unstable nature from the positive values.

Period	Number of UPOs
Period-1	1
Period-2	1
Period-3	1
Period-4	2
Period-5	4
Period-6	6

Table 1 – Number of Identified UPOs.

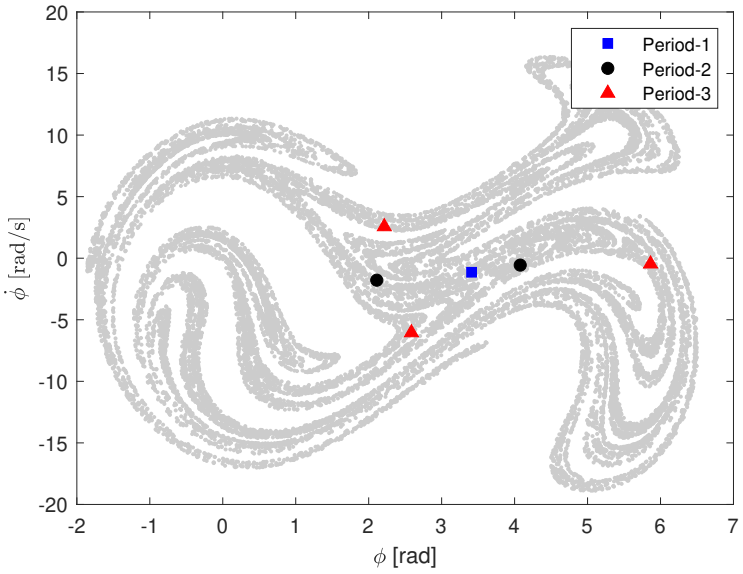

(a) Poincaré section;

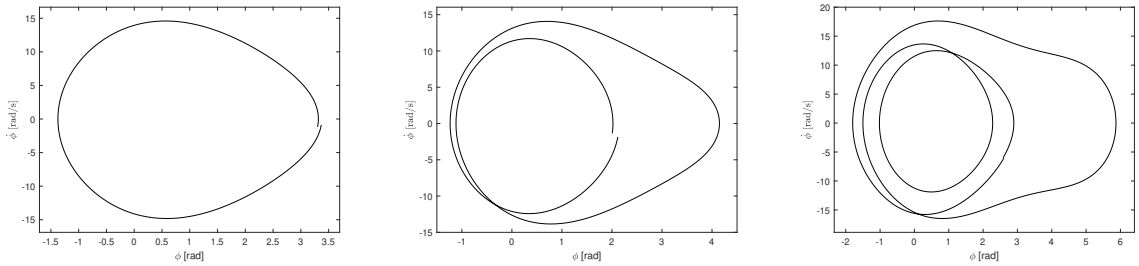

(b) Period-1 UPO; (c) Period-2 UPO; (d) Period-3 UPO;

Figure 5.1 – UPOs of the control rule.

Period	Lyapunov Exponent
1	1.531
2	1.411
3	0.638

Table 2 – Lyapunov exponent for selected UPOs without control.

5.2 Control Gains Evaluation

The second phase of the learning stage is the evaluation of the control gains from an analysis of the largest Lyapunov exponents of each UPO. This is the most computationally expensive part of the control process.

Different controller gains are considered in this phase. The evaluation is performed for values of $R = 0.0$, $R = 0.2$, and $R = 0.4$. Regarding the matrix $\mathbf{K}$, the gains K_{11}, K_{12}, K_{21}, and K_{22} are combined two by two and systematically varied from 0 to 2.5 with an increments of 0.1. Additionally, only the gain K_{22} is also considered, as is common in the literature, for comparison with the generalized ETDF.

The criterion for selection involves choosing values for R and $\mathbf{K}$ in order to minimize

the largest Lyapunov exponent. Minimal value of the largest Lyapunov exponent values provide faster convergence rates (PYRAGAS, 1995). Moreover, the choice of lower R and $\mathbf{K}$ values implies less modification to the system, which is desired for the control. Stabilizing higher periodicity UPOs tends to be more difficult, requiring greater values of R to achieve negative Lyapunov exponents (PAULA; SAVI, 2009a).

5.2.1 Period-1 UPO

Figures 5.2, 5.3, 5.5, 5.4, and 5.6 depict the maximum Lyapunov exponent of the period-1 UPO for different $\mathbf{K}$ values. Figure 5.2 shows the conventional approach with a scalar K for $R = 0.0$, $R = 0.2$, and $R = 0.4$ (PAULA; SAVI, 2009a; PAULA; SAVI, 2011). The selected gains are $R = 0.0$, $K = 1.9$, $\lambda = -0.448$, and it is represented with ○ in the Figure. Figures 5.3, 5.5, 5.4, and 5.6 are displayed as contour plots for the assessment of maximum Lyapunov exponents using 2 gains simultaneously at a time.

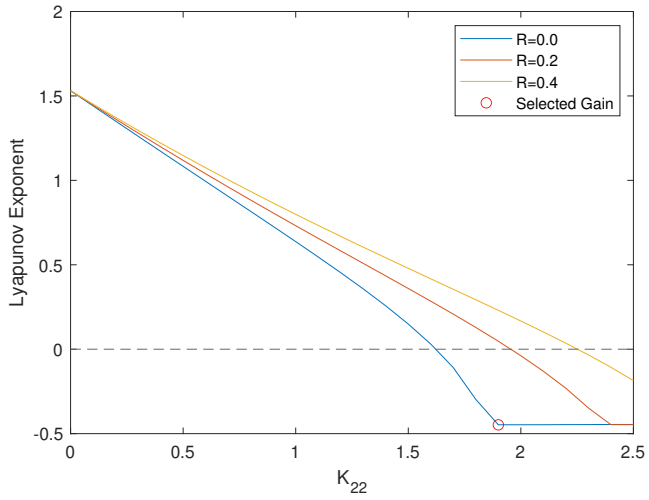

Figure 5.2 – Period-1 UPO largest Lyapunov exponent for scalar K with multiple R.

Figure 5.3 incorporates gains K_{11} and K_{12} in the analysis. We observe that at lower values of K_{12}, negative Lyapunov exponents are attained for higher values of the gain K_{11}. It's worth noting that these values surpass those associated with the conventional approach. Otherwise, an increase in K_{12} leads to an elevation of the Lyapunov exponent, making the orbit more unstable. The unstable behavior may be desired in specific situations, as when needed to change the UPO to be stabilized.

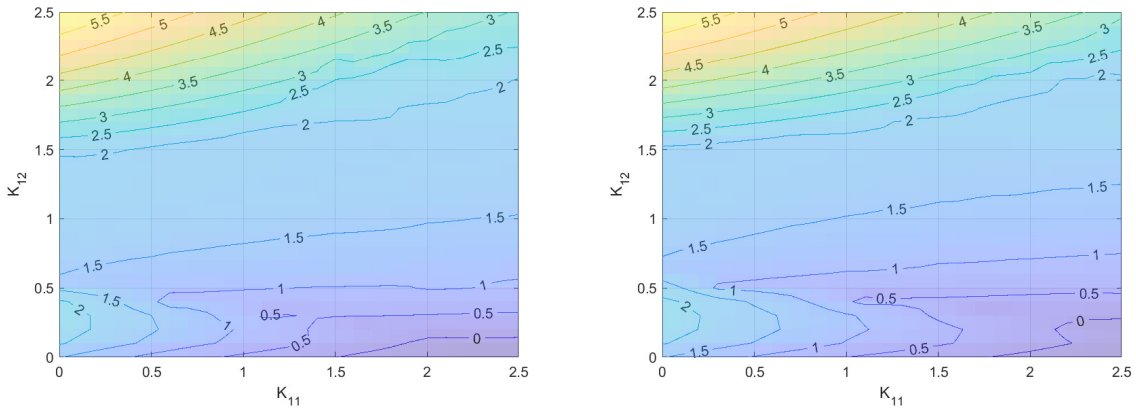

(a) $R = 0.0$.

(b) $R = 0.2$.

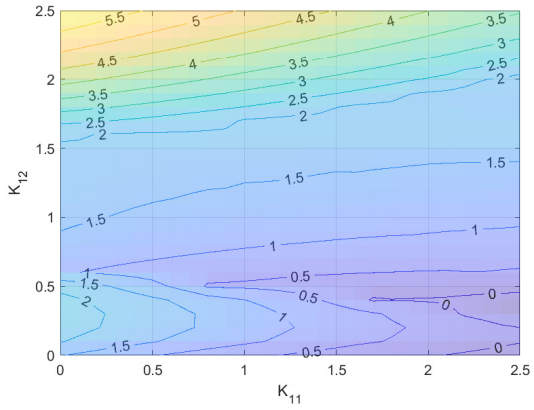

(c) $R = 0.4$.

Figure 5.3 – Period-1 UPO largest Lyapunov exponent for K_{11} and K_{12} and multiple R values.

The results obtained for K_{11} and K_{22} are presented in Figure 5.4. Both gains similarly influence the Lyapunov exponent values, consistently decreasing them. When both gains are elevated, the Lyapunov exponent increases. The region of negative values is more extensive than when compared to the case of a scalar gain. The area expands considerably when increasing the valor of R. The selected gains are $R = 0.0$, $K_{11} = 0.2$, $K_{22} = 1.8$ with $\lambda = -0.448$.

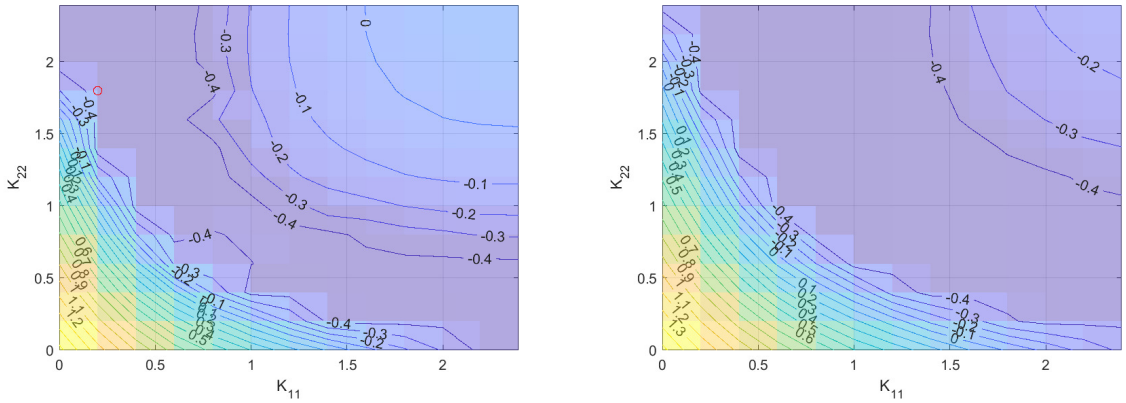

(a) $R = 0.0$.

(b) $R = 0.2$.

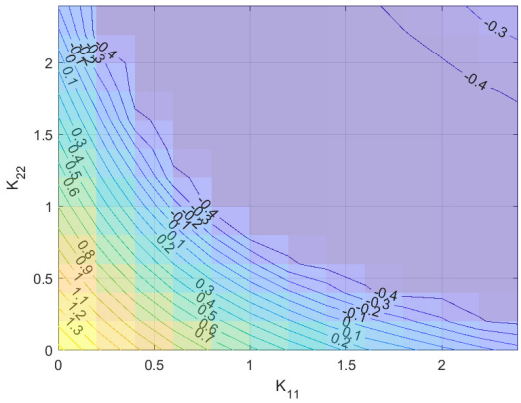

(c) $R = 0.4$.

Figure 5.4 – Period-1 UPO largest Lyapunov exponent for K_{11} and K_{22} and multiple R values.

Figure 5.5 depicts the Lyapunov exponent considering both K_{21} and K_{22}. Note that the minimum values of the maximum Lyapunov exponent are observed around $K_{21} = 1$. In comparison to the control system using only scalar gains, the generalized gain exhibits a more extensive region characterized by negative exponents. Moreover, the negative Lyapunov exponents regions became larger with higher values of R. The magnitude of the maximum Lyapunov exponent's minimum value is the same magnitude as the scalar approach. The selected gains are $R = 0.0$, $K_{21} = 0.2$, $K_{22} = 1.7$ with $\lambda = -0.284$, and it is represented with $\circ$ in the Figure.

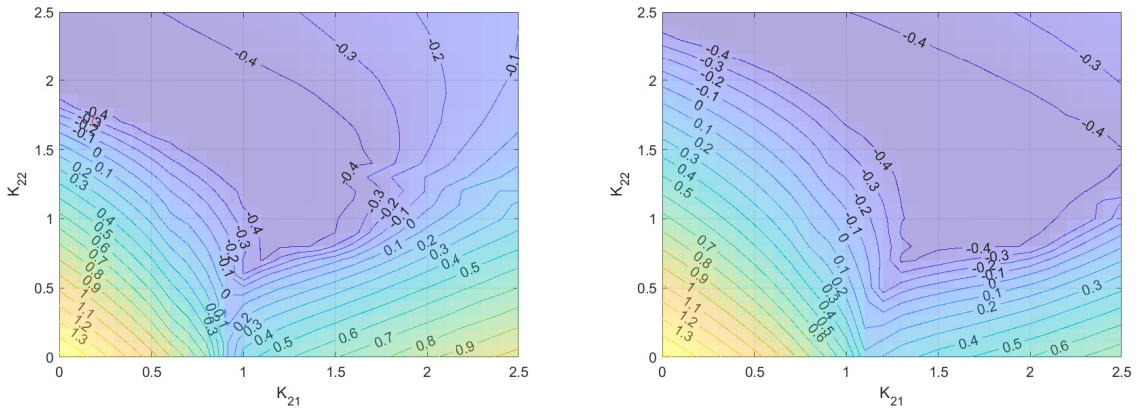

(a) $R = 0.0$.

(b) $R = 0.2$.

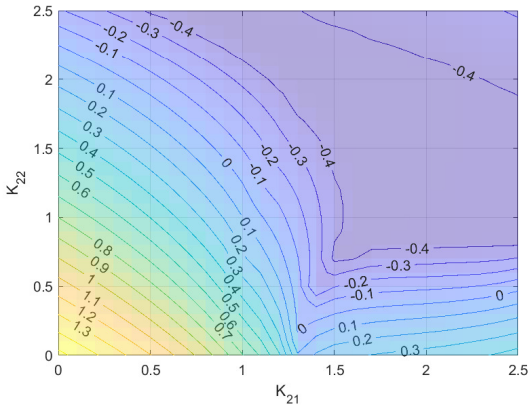

(c) $R = 0.4$.

Figure 5.5 – Period-1 UPO largest Lyapunov exponent for K_{21} and K_{22} and multiple R values.

Figure 5.6 presents the Lyapunov exponents when considering 3 gains of $\mathbf{K}$, with $K_{11} = 0.2$ and varying values for K_{21} and K_{22}. The magnitude of the exponent is consistent with other evaluations for this UPO. Employing the method using these 3 gains and $R = 0.4$ results in a larger region of negative exponents. The selected gains are $R = 0.0$, $K_{11} = 0.2$, $K_{21} = 0.2$, $K_{22} = 1.4$ with $\lambda = -0.442$, and it is represented with $\circ$ in the Figure.

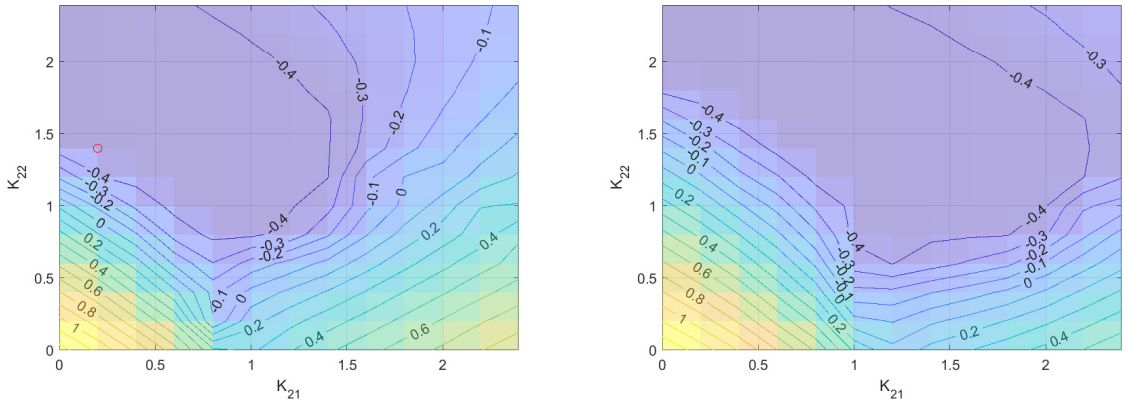

(a) $R = 0.0$.

(b) $R = 0.2$.

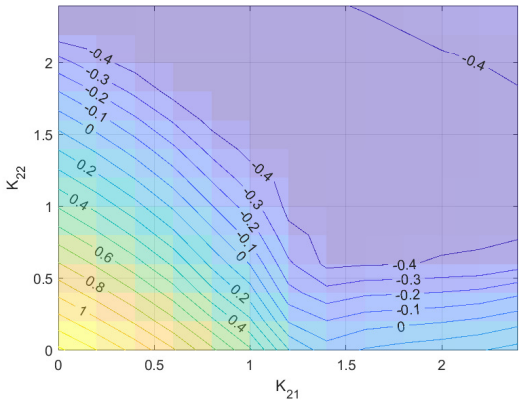

(c) $R = 0.4$.

Figure 5.6 – Period-1 UPO largest Lyapunov exponent for $K_{11} = 0.2$, varying K_{21} and K_{22} and multiples R.

5.2.2 Period-2 UPO

Similarly to the analysis of the period-1 UPO, Figures 5.7, 5.8, 5.10, 5.9, and 5.11 depict the maximum Lyapunov exponents for the period-2 UPO considering different **K** values. The approach with a scalar K is shown in Figure 5.7. no K value yields negative exponents for this UPO when $R = 0.0$. However, negative values are observed for both $R = 0.2$ and $R = 0.4$. The selected gains are $R = 0.2$, $K = 1.2$ with $\lambda = -0.108$, and it is represented with ○ in the Figure.

Figure 5.8 refers to the Lyapunov exponents when analysing gains K_{11} and K_{12} for period-2 UPO. Similarly to the period-1 orbit, the increasing gain K_{12} made it more unstable, with higher Lyapunov exponents. gain K_{11} had a small influence on the system stability, though it could make a small region of negative exponents by itself with $R = 0.4$.

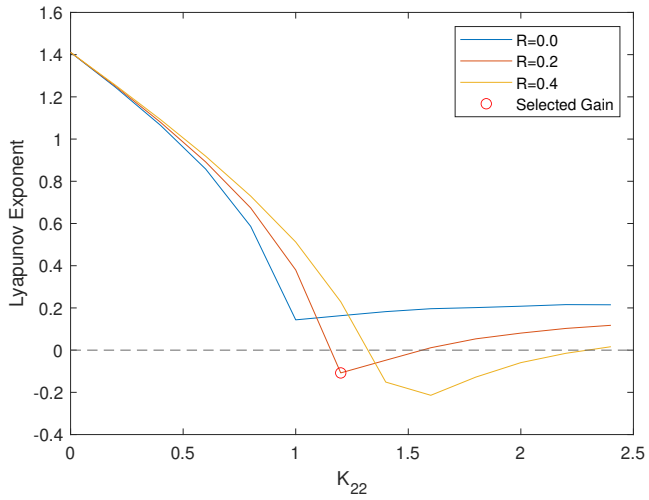

Figure 5.7 – Period-2 UPO largest Lyapunov exponent for scalar K with multiple R.

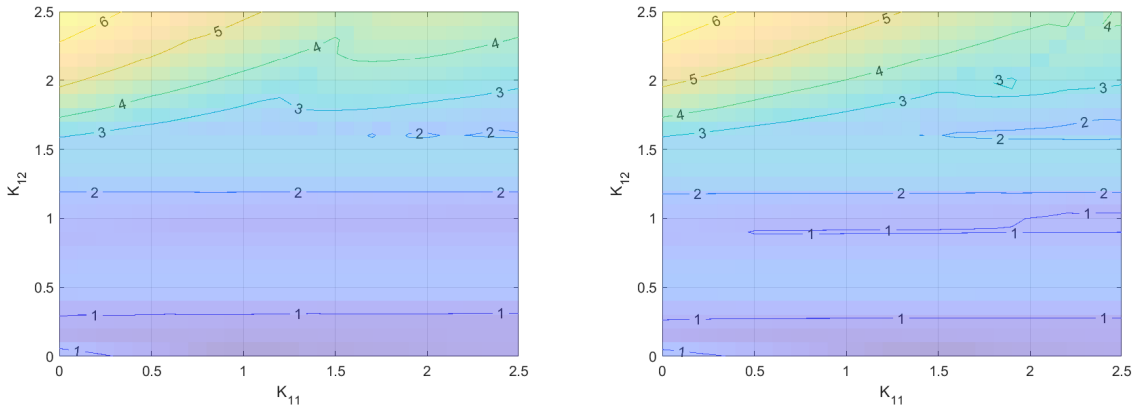

(a) $R = 0.0$.

(b) $R = 0.2$.

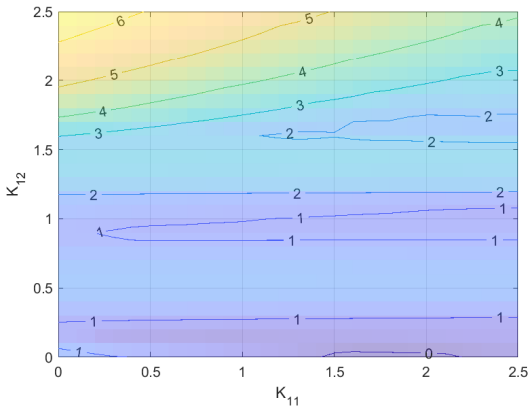

(c) $R = 0.4$.

Figure 5.8 – Period-2 UPO largest Lyapunov exponent for K_{11} and K_{12} and multiple R values.

The Lyapunov exponents for K_{11} and K_{22} is shown in Figure 5.9. Unlike K_{22}, K_{11} gain cannot make the orbit stable by itself. When considering $R = 0.2$, minimum values of the maximum Lyapunov exponent are observed around $K_{22} = 1.2$ when considering

it individually. The combination of both K_{11} and K_{22} made a the minimal values of the exponent observed around $K_{11} = 0.2$ and $K_{22} = 1.0$, reducing the K_{22} magnitude. This combination achieved lower Lyapunov exponents than the scalar approach. Moreover, the region of negative exponents is larger than the case with scalar gain. The selected gains are $R = 0.2$, $K_{11} = 0.2$, $K_{22} = 1.0$ with $\lambda = -0.152$, and it is represented with ○ in the Figure.

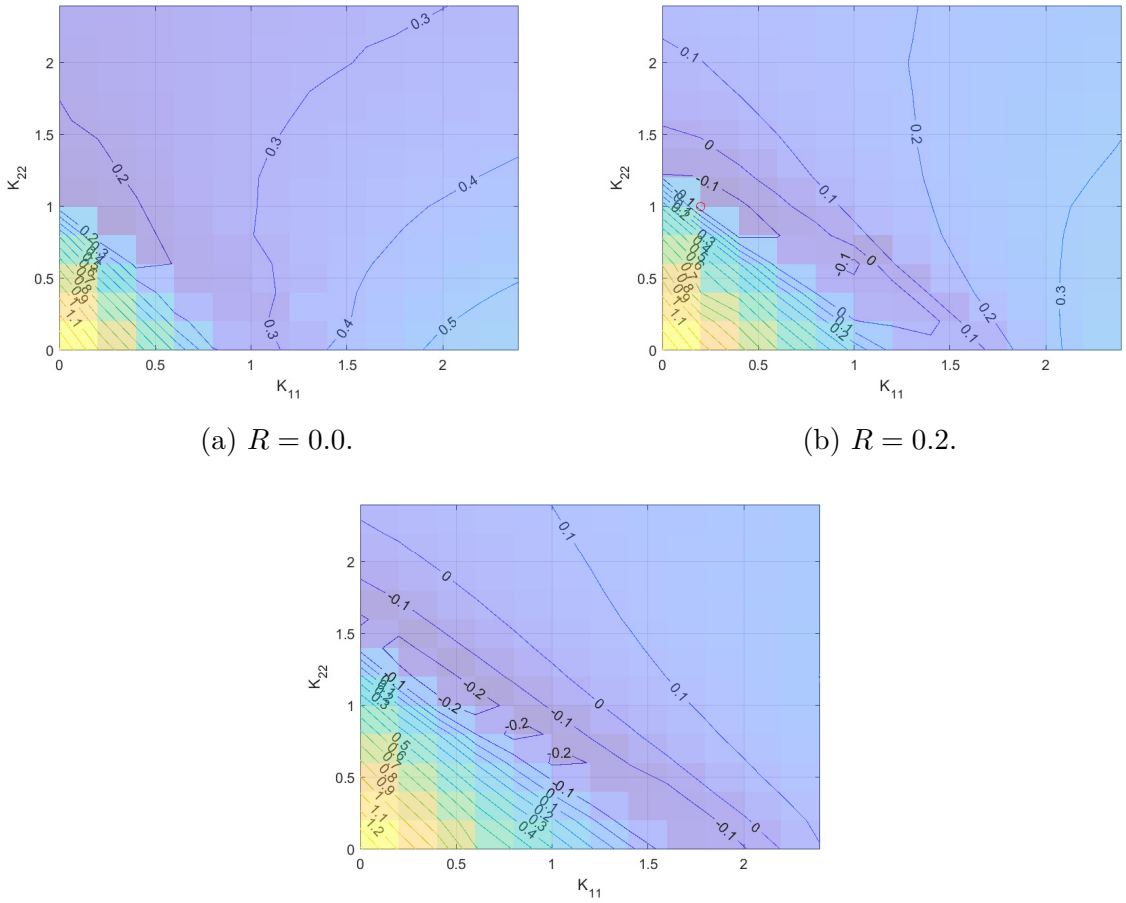

(a) $R = 0.0$.

(b) $R = 0.2$.

(c) $R = 0.4$.

Figure 5.9 – Period-2 UPO largest Lyapunov exponent for K_{11} and K_{22} and multiple R values.

Figure 5.10 incorporates the Lyapunov exponents analysis for K_{21} and K_{22}. To achieve stability conditions for the system, values of $R = 0.2$ or $R = 0.4$ were required. The gain K_{22} had a greater influence on decreasing the Lyapunov exponent. K_{21} could not reach a stable condition by itself, but combined with K_{22}, it attains lower values. A combined use of the gains allowed a greater range for negative values of the Lyapunov exponent. The selected gains are $R = 0.2$, $K_{21} = 0.7$, $K_{22} = 1.2$ with $\lambda = -0.162$, and it is represented with ○ in the Figure.

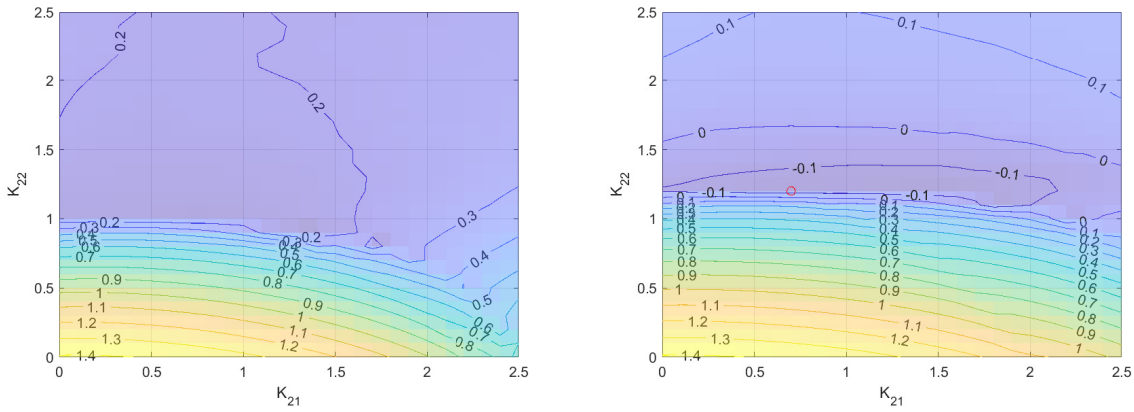

(a) $R = 0.0$.

(b) $R = 0.2$.

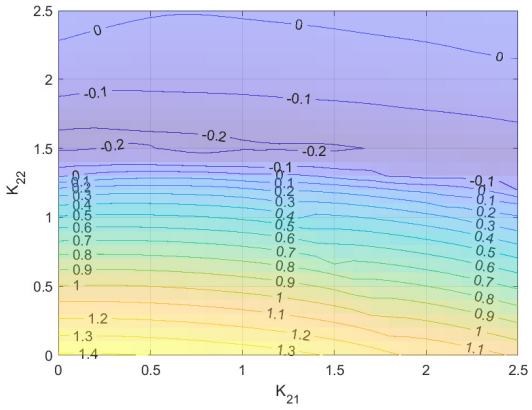

(c) $R = 0.4$.

Figure 5.10 – Period-2 UPO largest Lyapunov exponent for K_{21} and K_{22} and multiple R values.

Figure 5.11 demonstrate the Lyapunov exponents when considering 3 gains of $\mathbf{K}$, multiples values for multiple values for K_{21} and K_{22} and $K_{11} = 0.4$. This combination of gains achieved lower Lyapunov exponent values than the scalar and 2-gains evaluations. The selected gains are $R = 0.2$, $K_{11} = 0.4$, $K_{21} = 0.4$, $K_{22} = 0.8$ with $\lambda = -0.192$, and it is represented with $\circ$ in the Figure.

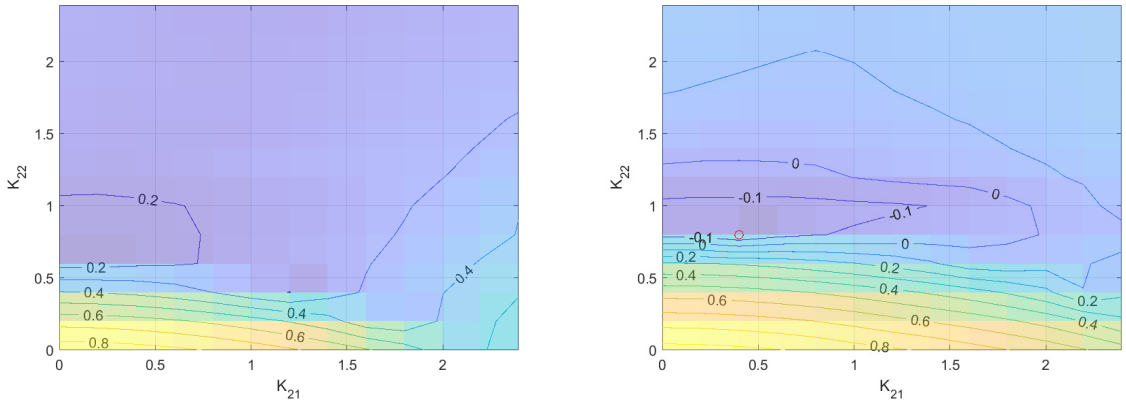

(a) $R = 0.0$.

(b) $R = 0.2$.

(c) $R = 0.4$.

Figure 5.11 – Period-2 UPO largest Lyapunov exponent for $K_{11} = 0.4$, varying K_{21} and K_{22} and multiples R.

5.2.3 Period-3 UPO

Similarly to the analysis of the period-1 and period-2, period-3 UPO study is shown in Figures 5.12, 5.13, 5.15, 5.14, and 5.16 for various **K** configurations.

The approach with a scalar K is depicted in Figure 5.12. The scalar approach reaches negative Lyapunov exponents for all R values. The selected gains are $R = 0.2$, $K = 0.6$ with $\lambda = -0.198$, and it is represented with ○ in the Figure.

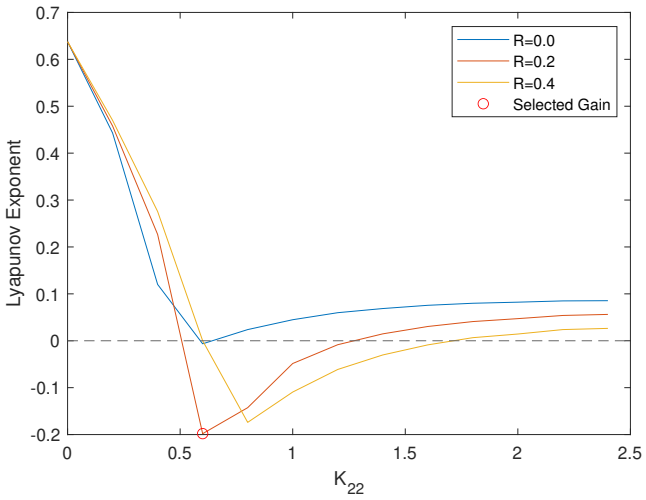

Figure 5.12 – Period-3 UPO largest Lyapunov exponent for scalar K with multiple R.

Figure 5.13 represents the Lyapunov exponent when assessing both K_{11} and K_{12} values for various R values. Similarly to the period-1 and 2 UPOs, K_{12} acted by increasing the Lyapunov exponent. On the other side, K_{11} had a little impact on the exponent, it managed to make it a negative for a small area for each R evaluated, but only for near zero values.

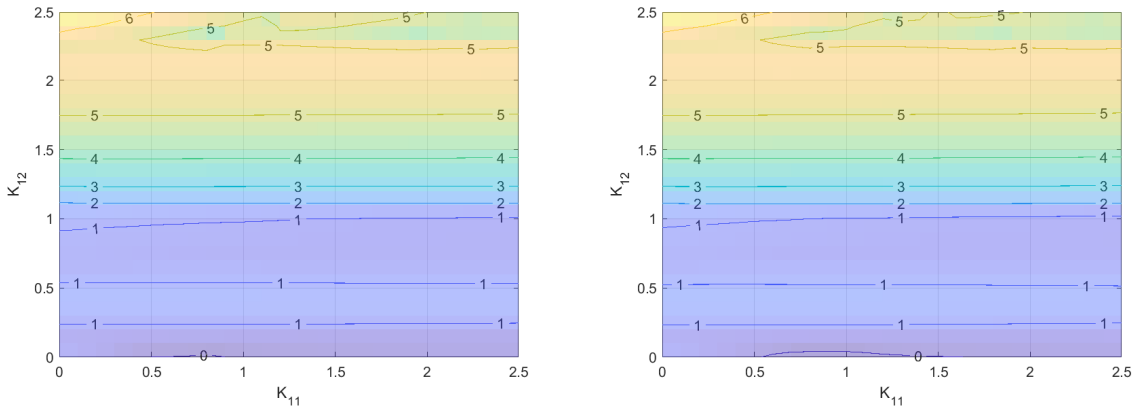

(a) $R = 0.0$.

(b) $R = 0.2$.

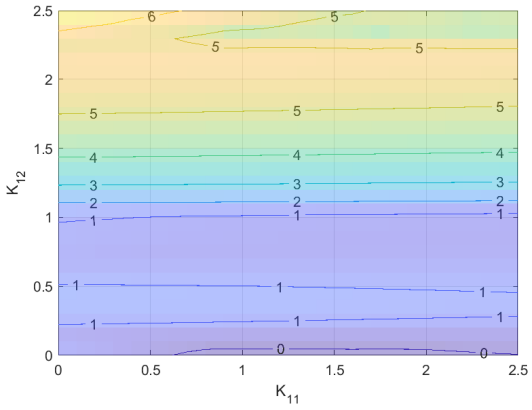

(c) $R = 0.4$.

Figure 5.13 – Period-3 UPO largest Lyapunov exponent for K_{11} and K_{12} and multiple R values.

The evaluation for both K_{11} and K_{22} is shown in Figure 5.14. K_{11} reached negative values for the Lyapunov exponent by itself, as did K_{22}. The K_{11} gain had more influence in decreasing the exponent when compared to K_{22}. The combination of both gains leads to a region for negative exponents with lower values than when considering the scalar K. The selected gains are $R = 0.2$, $K_{11} = 0.4$, $K_{22} = 0.4$ with $\lambda = -0.202$, and it is represented with $\circ$ in the Figure.

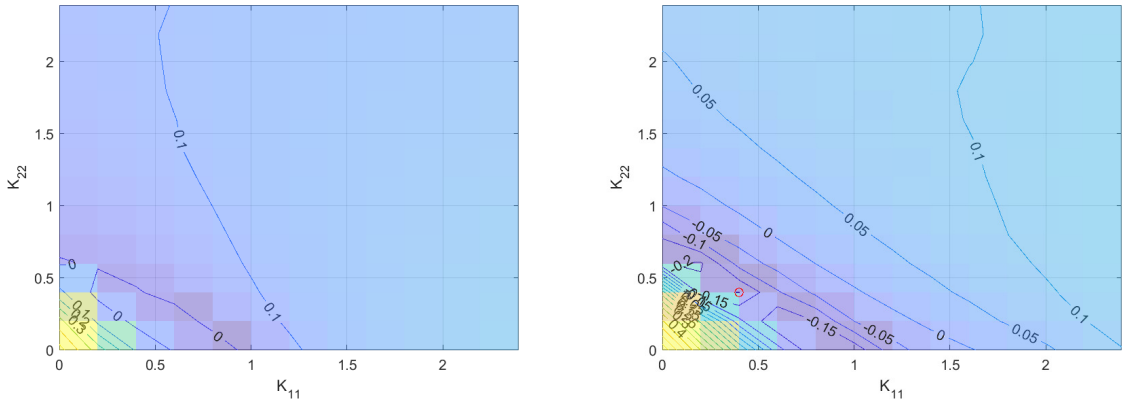

(a) $R = 0.0$.

(b) $R = 0.2$.

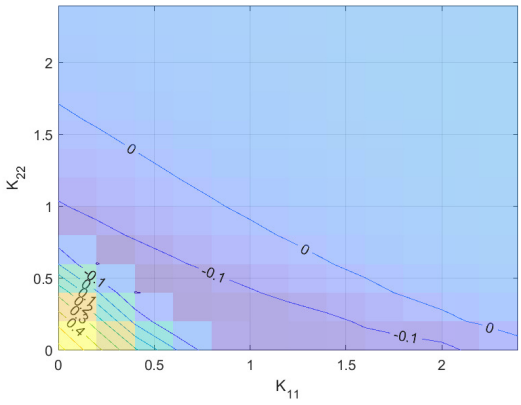

(c) $R = 0.4$.

Figure 5.14 – Period-3 UPO largest Lyapunov exponent for K_{11} and K_{22} and multiple R values.

Figure 5.15 shows Lyapunov exponents for period-3 UPO when considering K_{21} and K_{22}. Different from period-1 and similarly to period-2 UPOs, K_{21} had a lesser impact in decreasing Lyapunov exponents. It made a bigger area of negative value, and they were smaller than the scalar approach. The selected gains are $R = 0.2$, $K_{21} = 0.4$, $K_{22} = 0.6$ with $\lambda = -0.189$, and it is represented with $\circ$ in the Figure.

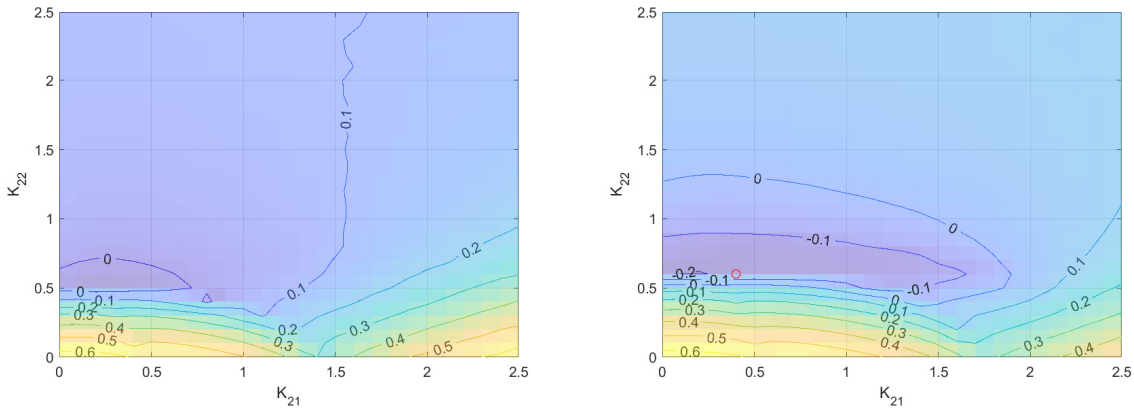

(a) $R = 0.0$.

(b) $R = 0.2$.

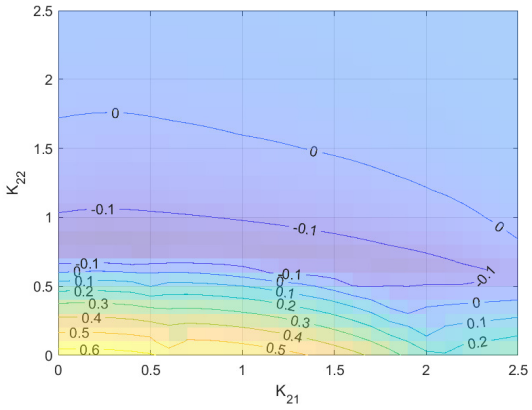

(c) $R = 0.4$.

Figure 5.15 – Period-3 UPO largest Lyapunov exponent for K_{21} and K_{22} and multiple R values.

Figure 5.16 evaluates the maximum Lyapunov exponent considering $K_{11} = 0.2$, and varying K_{21} and K_{22}. The negative exponent area is increased when compared with the situation where $K_{11} = 0$, Figure 5.15, for the correspondent value of R. Despite the area increase, the exponents values have the same order of magnitude. The selected gains are $R = 0.2$, $K_{11} = 0.2$, $K_{21} = 0.4$, $K_{22} = 0.6$ with $\lambda = -0.194$, and it is represented with ○ in the figure.

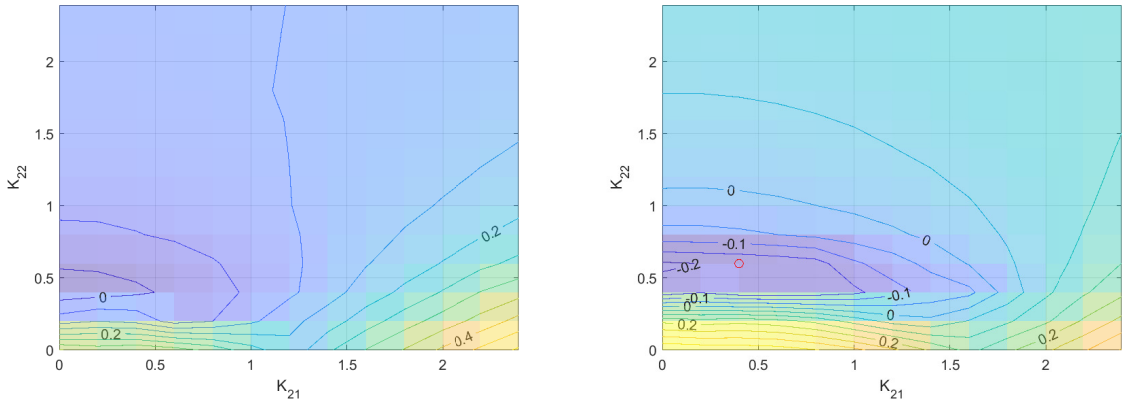

(a) $R = 0.0$.

(b) $R = 0.2$.

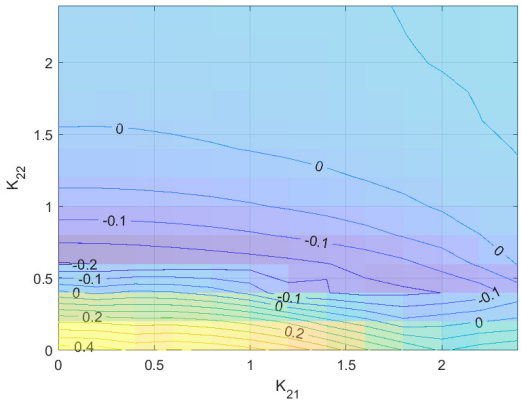

(c) $R = 0.4$.

Figure 5.16 – Period-3 UPO largest Lyapunov exponent for $K_{11} = 0.2$, varying K_{21} and K_{22} and multiples R.

5.2.4 Selected Gains

Four different combinations of gains were selected for stabilizing each unstable periodic orbit. The classical approach with scalar gain $K = K_{22}$, and situations with both K_{21} and K_{22}; both K_{11} and K_{22}; and with K_{11}, K_{21}, and K_{22}. The chosen values for the controller gains for scalar and matrix $\mathbf{K}$ are shown in Tables 3 and 4, respectively.

Period	R	K_{22}	Lyapunov Exponent
1	0.0	1.9	-0.448
2	0.2	1.2	-0.108
3	0.2	0.6	-0.198

Table 3 – Selected gains for control with scalar K and respective value of maximum Lyapunov Exponents.

Period	R	K_{11}	K_{12}	K_{21}	K_{22}	Lyapunov Exponent
1	0.0	0.0	0.0	0.2	1.7	-0.284
1	0.0	0.2	0.0	0.0	1.8	-0.448
1	0.0	0.2	0.0	0.2	1.4	-0.442
2	0.2	0.0	0.0	0.7	1.2	-0.152
2	0.2	0.2	0.0	0.0	1.0	-0.162
2	0.2	0.4	0.0	0.4	0.8	-0.192
3	0.2	0.0	0.0	0.4	0.6	-0.189
3	0.2	0.4	0.0	0.0	0.4	-0.202
3	0.2	0.2	0.0	0.4	0.6	-0.194

Table 4 – Selected gains for control with matrix **K** and respective maximum Lyapunov Exponents.

6 Stabilization Stage

This chapter presents the results of the stabilization stage when small perturbations are imposed to the system to stabilize one of its UPOs.

The controller performance is evaluated by considering the following criteria: UPO stabilization time, energy required for stabilization, and maximum perturbation of Δl, related to B_2 actuation. The stabilization time is evaluated by considering the Euclidean distance between $\dot{\phi}$ and $\ddot{\phi}$ of the reference orbits and the controlled trajectory. A threshold of the Euclidean distance is stipulated, being dis = 1 for the period-1 UPO and dis = 3 for period-2 and period-3 UPOs.

The controller energy consumption is estimated for both B_1 and B_2 actuation. In the case of B_1, the instantaneous power is computed as $\text{Pot}_{\text{inst}} = B_1 I\ddot{\phi}$. Power consumption for B_2 is obtained from the torques applied by the controller B_2, $\tau = \frac{kd}{2}\Delta l$, being computed as $P = \tau\dot{\phi}$. Energy consumption is determined by integrating the sum of the instantaneous power of each actuation term over time.

This study provides a comparative analysis of control performance employing two different approaches: the reference case, characterized by the classical scalar gain $K = K_{22}$ commonly used in the literature (PAULA; SAVI, 2009a; PAULA; SAVI, 2011), and the generalized ETDF control. The matrix gain $\mathbf{K}$ is examined across three scenarios: using both K_{21} and K_{22} where only B_2 action occurs; using both K_{11} and K_{22} which means that the control action has both B_1 and B_2; and using K_{11}, K_{21} and K_{22}. The gain K_{12} is not considered because it destabilizes the UPOs, as evidenced by the evaluation of maximum Lyapunov exponents.

6.1 Period-1 UPO Stabilization

Figure 6.1 shows the stabilization results for the period-1 UPO with K_{21} and K_{22} compared with the reference case. Sub-figure (a) depicts the target UPO in black and phase space in steady regime obtained from both controls evaluated; Sub-figure (b) shows the control signal in time; and Sub-figure (c) shows the instantaneous power control consumption. Blue lines refer to scalar K approach, and the red ones are associated with the generalized ETDF. Nevertheless, control signals are similar in both strategies; the

energy consumption is lower in when both gains are used simultaneously. The total energy consumption of actuators is $E = 34.4$ J for a scalar gain and $E = 29.3$ for generalized control. The stabilization with $\mathbf{K}$ presents a maximum actuation value of $\Delta l = 117.6$ mm while the scalar gain K presents $\Delta l = 129.4$ mm. Therefore, incorporating both gains enables the system to be stabilized at a similar time when compared to the reference case but with smaller maximum actuation and smaller energy consumption.

Some other combinations of K_{21} and K_{22} are able to stabilize the pendulum within less time or with a smaller actuation than considering only the scalar gain; therefore, it increases possible control gain choices, bringing more flexibility to the controller.

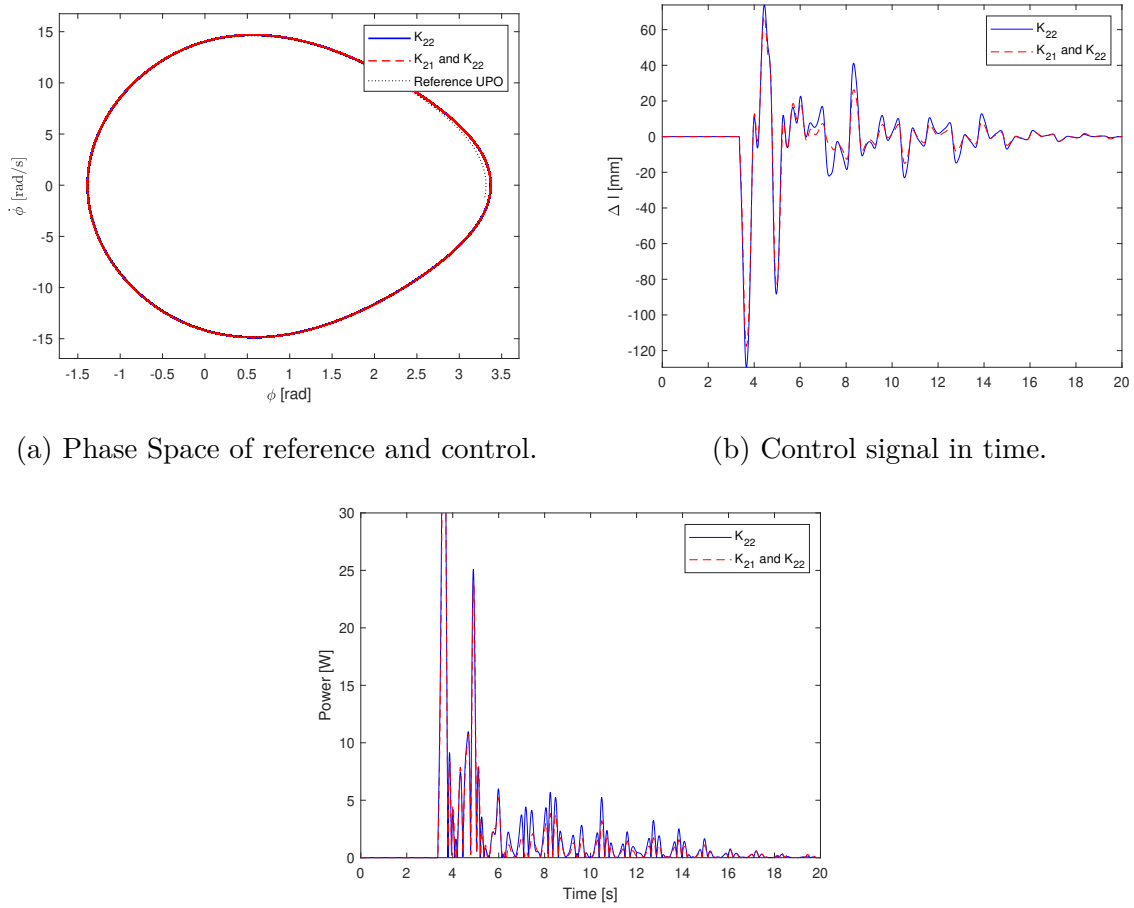

(a) Phase Space of reference and control.

(b) Control signal in time.

(c) Power consumed by control action.

Figure 6.1 – Period-1 UPO control comparison of scalar K with both K_{21} and K_{22}.

Figure 6.2 reveals similar results to the previous analysis for generalized ETDF with K_{11} and K_{22}. Sub-figures 6.2b and 6.2c present both B_1 and B_2 control action and its power consumption separately. The stabilization time for the scalar K was of $t = 14.1$ s, while for K_{11} and K_{22} it reduced to $t = 9.7$ s, 31% decrease. The maximum actuation for the matrix approach for B_2 control was $\Delta l = 119.6$ mm, approximately 7% less than the scalar reference. The total energy consumption amounted to $E = 30.4$ J, reflecting 11% less than the reference control.

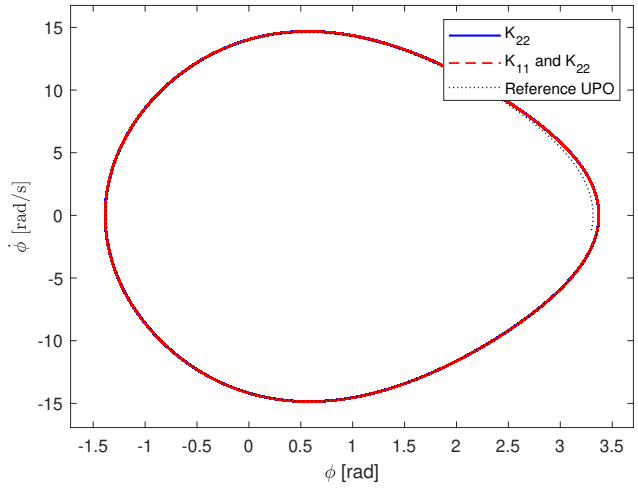

(a) Phase Space of reference and control.

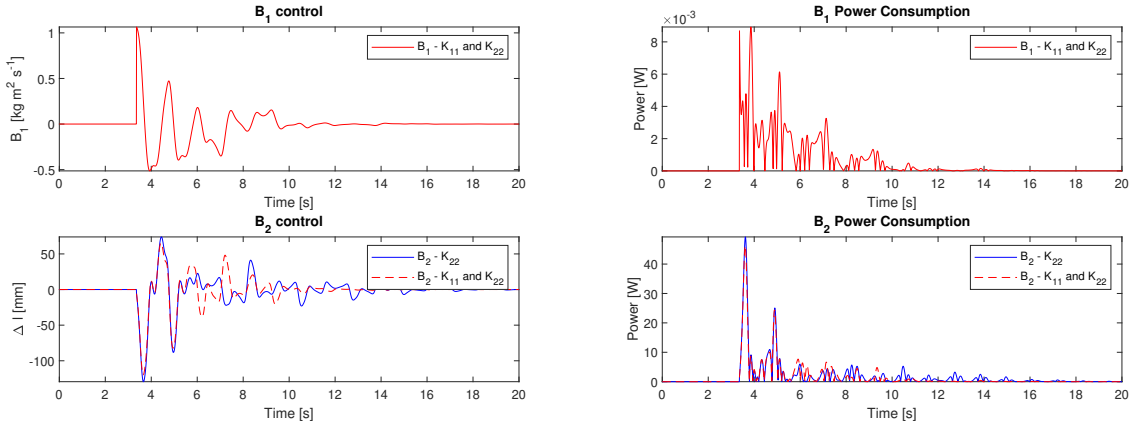

(b) Control signal in time.

(c) Power consumed by control action.

Figure 6.2 – Period-1 UPO control comparison of scalar K with both K_{11} and K_{22}.

Period-1 UPO stabilization comparing scalar K to when using three gains on $\mathbf{K}$ is presented in Figure 6.3. The maximum actuation of the matrix approach was $\Delta l = 96.5$ mm, 25% less than the scalar. Otherwise, the energy consumption was $E = 42.8$ J and time until stabilization $t = 18.5$ s, both higher than the scalar situation. This situation is better suited for situations with a lower actuation and when energy and time are not priorities.

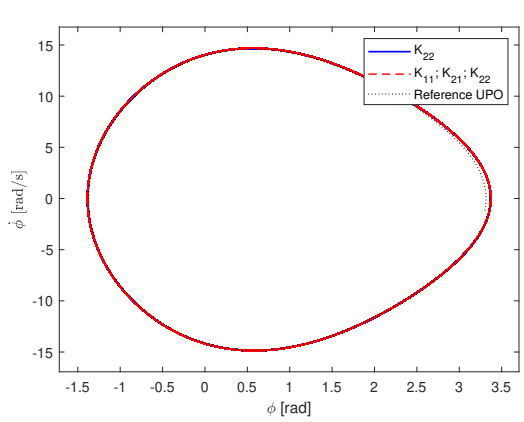

(a) Phase Space of reference and control.

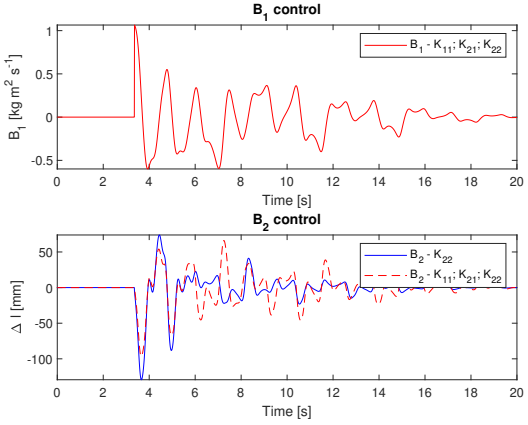

(b) Control signal in time.

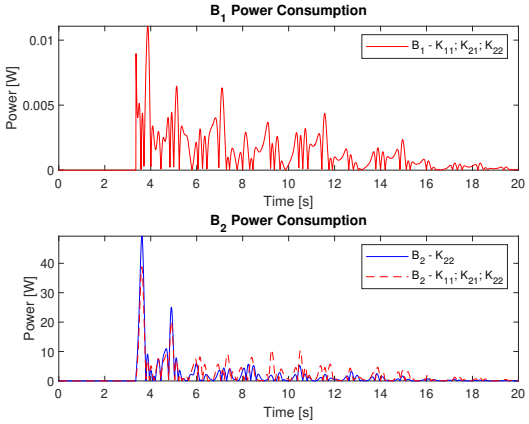

(c) Power consumed by control action.

Figure 6.3 – Period-1 UPO control comparison of scalar K with K_{11}, K_{21}, and K_{22}.

6.2 Period-2 UPO Stabilization

Figure 6.4 compares the scalar approach with when using K_{21} and K_{22} on $\mathbf{K}$ for period-2 UPO. The scalar approach had a maximum actuation of $\Delta l = 77.1$ mm, consumed $E = 45.5$ J to stabilize the reference UPO. When considering K_{21} and K_{22}, the system was stabilized with $\Delta l = 81.5$ mm and consumed $E = 59.8$ J. This approach used 2 gains related to B_2 control. These values were $K_{21} = 0.7$ and $K_{22} = 1.2$, influencing the control to have bigger actuation. This resulted in greater actuation and consumption than the conventional approach.

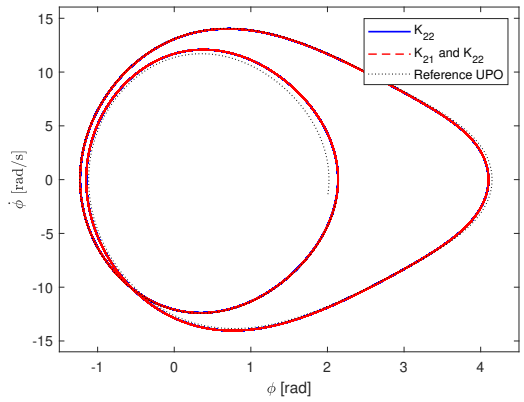

(a) Phase Space of reference and control.

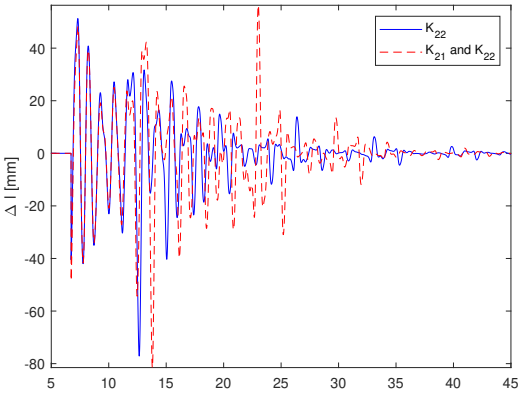

(b) Control signal in time.

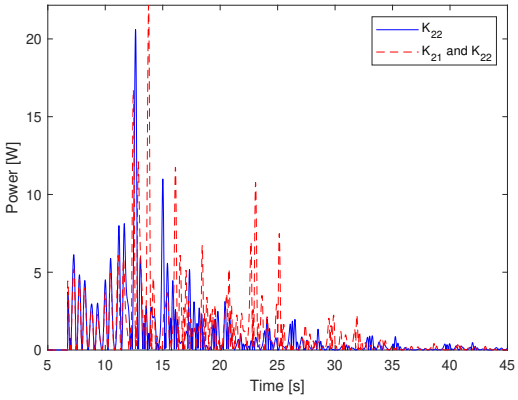

(c) Power consumed by control action.

Figure 6.4 – Period-2 UPO control comparison of scalar K with both K_{21} and K_{22}.

Period-2 control using K_{11} and K_{22} is shown in Figure 6.5. This configuration used a maximum actuation of $\Delta l = 60.1$ mm, 22 % of the scalar approach. On the other hand, it consumed $E = 47.4$ J, about the same as the reference.

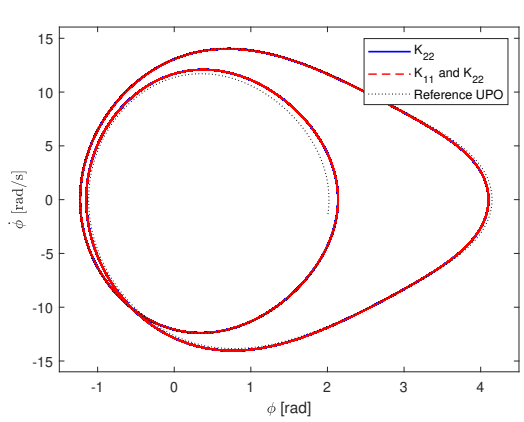

(a) Phase Space of reference and control.

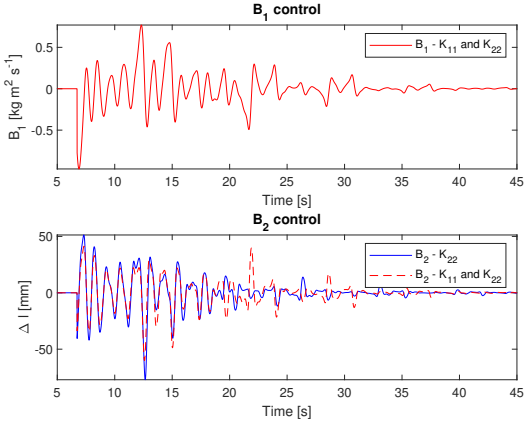

(b) Control signal in time.

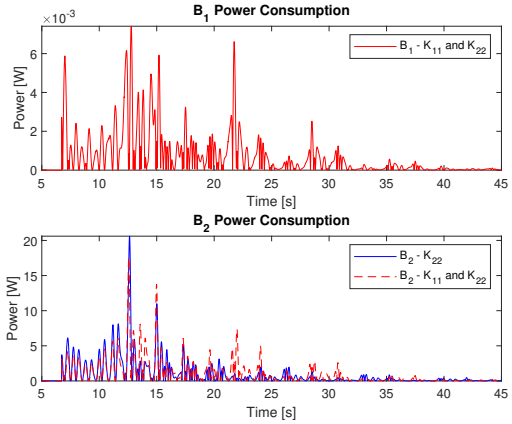

(c) Power consumed by control action.

Figure 6.5 – Period-2 UPO control comparison of scalar K with both K_{11} and K_{22}.

Figure 6.6 brings the period-2 UPO control considering K_{11}, K_{21}, and K_{22}. The stabilization occurred with a maximum actuator displacement of $\Delta l = 54.2$ mm, 29,7 % less than the scalar. The energy consumption was $E = 40.8$ J, about 10% smaller. This configuration of 3 elements in $\mathbf{K}$ could achieve a smaller Lyapunov exponent with smaller gains values. The smaller gains are related to the actuation intensity and energy consumption. The use of 3 gains in the controller made possible the choice of smaller gains with a higher convergence rate related to the Lyapunov exponent.

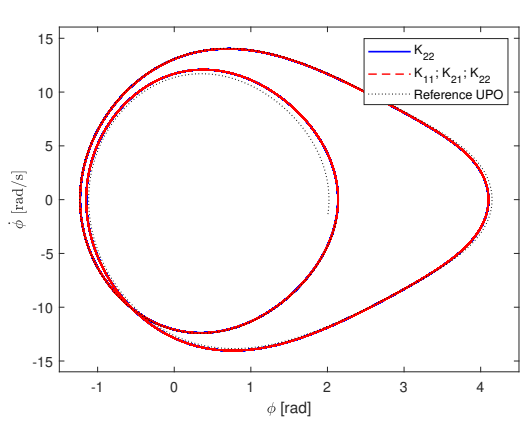

(a) Phase Space of reference and control.

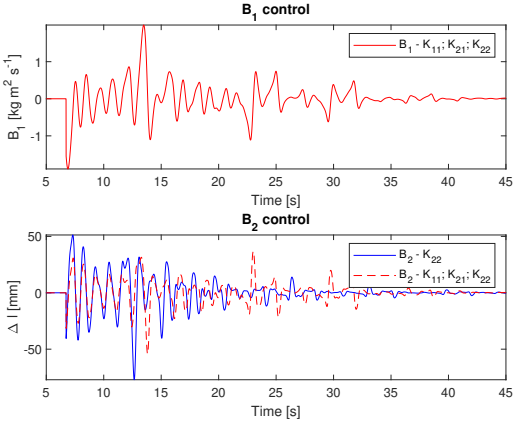

(b) Control signal in time.

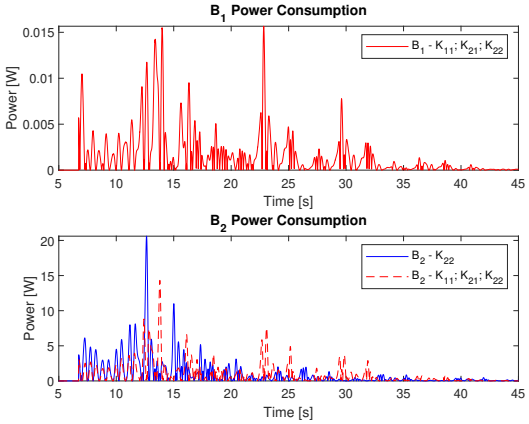

(c) Power consumed by control action.

Figure 6.6 – Period-2 UPO control comparison of scalar K with K_{11}, K_{21}, and K_{22}.

6.3 Period-3 UPO Stabilization

The period-3 UPO stabilization comparison between a scalar K and using both K_{21} and K_{22} is shown in Figure 6.7. The scalar approach had a maximum actuation of $\Delta l = 40.6$ mm and an energy consumption of $E = 40.6$ J. On the other hand, the matrix approach had a maximum actuation of $\Delta l = 40.4$ mm and energy consumption of $E = 35.2$ J. While the maximum actuation of both was very similar, it had 13% less energy consumption, and the stabilization was achieved faster.

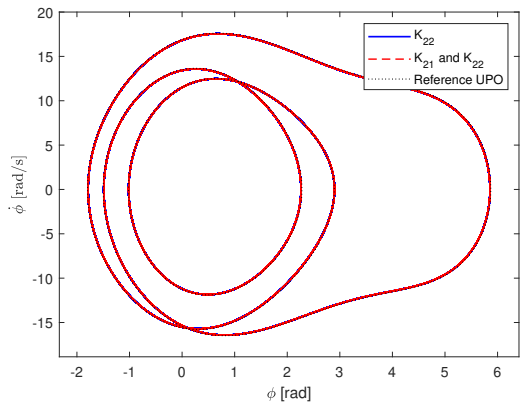

(a) Phase Space of reference and control.

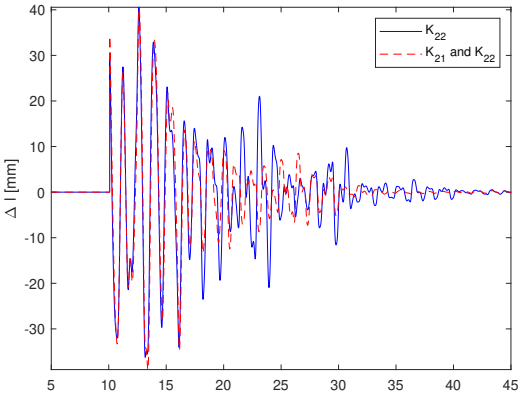

(b) Control signal in time.

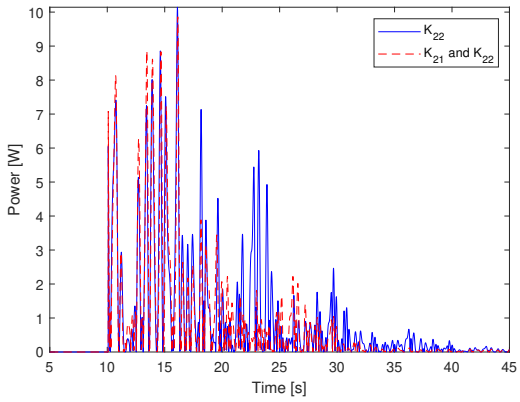

(c) Power consumed by control action.

Figure 6.7 – Period-3 UPO control comparison of scalar K with both K_{21} and K_{22}.

Figure 6.8 is related to the use of K_{11} and K_{22} gains on the control. This approach had the smaller maximum actuation of all period-3 with $\Delta l = 27.2$ mm, 33 % less than the scalar one. It also had a smaller energy consumption with $E = 23.2$ J, 43 % smaller. Furthermore, it was able to stabilize the desired orbit in less time.

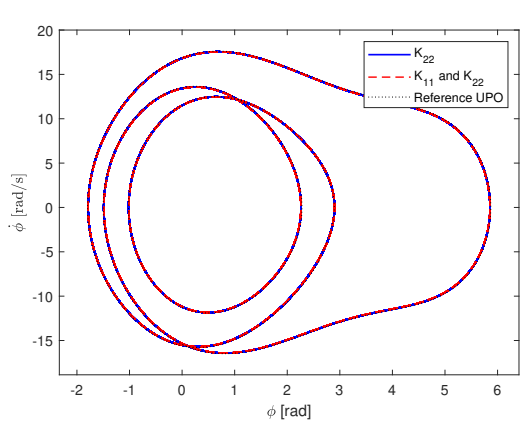

(a) Phase Space of reference and control.

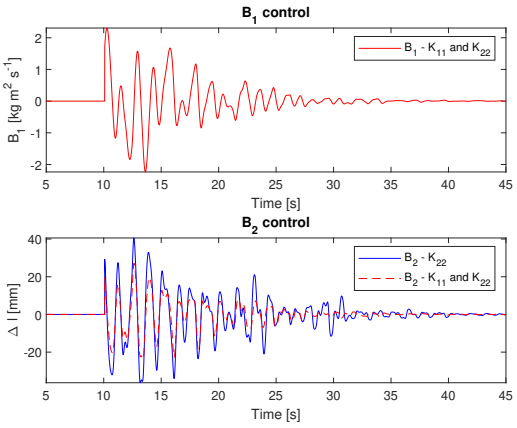

(b) Control signal in time.

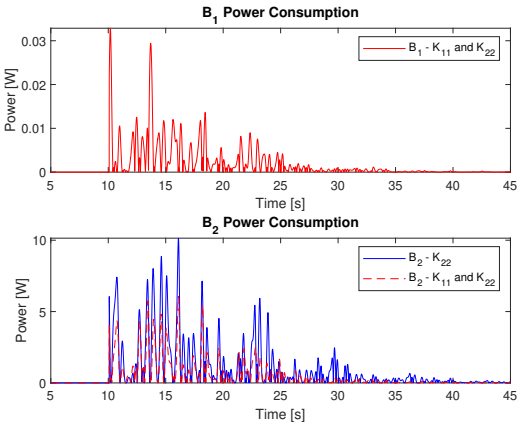

(c) Power consumed by control action.

Figure 6.8 – Period-3 UPO control comparison of scalar K with both K_{11} and K_{22}.

Stabilization using K_{11}, K_{21}, and K_{22} is shown in Figure 6.9. The phase space of the matrix form, Sub-figure 6.9a, has a wider band showing that the control is not precisely on the reference UPO. Despite this, the stabilization with three gains had a similar actuation to the scalar one with $\Delta l = 40.3$ mm. Otherwise, energy consumption was higher with $E = 41.7$ J. Since perfect stabilization was not achieved, the control consumption was impacted.

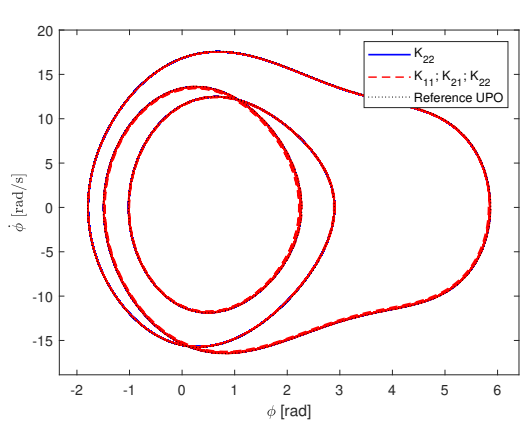

(a) Phase Space of reference and control.

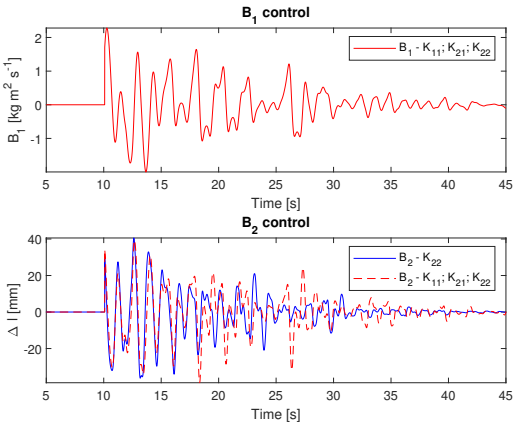

(b) Control signal in time.

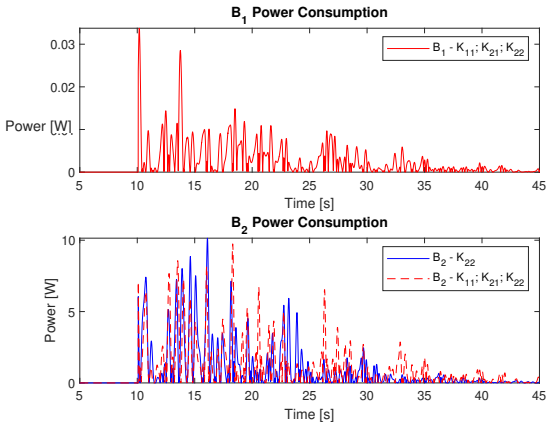

(c) Power consumed by control action.

Figure 6.9 – Period-3 UPO control comparison of scalar K with K_{11}, K_{21}, and K_{22}.

6.4 Control Performance Comparison

This section presents a comparative analysis of the generalized ETDF control performance for the different combinations of control gains employed to control chaos in the nonlinear pendulum. Initially, a baseline is defined with the conventional scalar approach. Following this, the control strategy incorporates various control gains of the **K** matrix.

Table 5 provides a summary of control performance in stabilizing the three orbits, considering different combinations of control gains.

Period	R	K_{11}	K_{21}	K_{22}	Lyapunov Exponent	Δl_{max} [mm]	B_1 Control Energy [mJ]	B_2 Control Energy [J]
1	0.0			1.9	-0.448	129.4		34.4
1	0.0		0.2	1.7	-0.284	117.6		29.3
1	0.0	0.2		1.8	-0.448	119.6	11.2	30.4
1	0.0	0.2	0.2	1.4	-0.442	96.5	22.9	42.8
2	0.2			1.2	-0.108	77.1		45.4
2	0.2		0.7	1.2	-0.152	81.5		59.8
2	0.2	0.2		1.0	-0.162	60.1	32.2	47.5
2	0.2	0.4	0.4	0.8	-0.192	54.2	68.9	40.7
3	0.2			0.6	-0.198	40.6		41.0
3	0.2		0.4	0.6	-0.189	40.5		35.2
3	0.2	0.4		0.4	-0.202	40.3	49.9	41.6
3	0.2	0.2	0.4	0.6	-0.194	27.2	81.2	23.1

Table 5 – Comparison of control performance for different sets of control gains.

The control using both K_{21} and K_{22} exhibited higher energy consumption for the period-1 and period-2 UPOs but a smaller consumption for the period-3 UPO. The combination of 2 gains generally results in decreased control actuation and, therefore, lowers energy consumption. Period-2 UPO control featured a higher value of the K_{21} gain in comparison to the other orbits, which lead to a bigger energy consumption and actuation. The introduction of a second gain makes the control more versatile, providing more options to prioritize either faster stabilization or energy consumption.

The approach considering both K_{11} and K_{22} had a similar total energy consumption to the baseline in all 3 cases. The maximum actuation was smaller in both period-1 and 2 UPOs. Stabilization was achieved faster in all evaluated orbits. The energy consumption related to the B_1 control action evaluated is around 1000 times less than the B_2.

6.5 Control Rule

In this section, a control rule, considering the sequential stabilization of the three UPOs, is employed to verify the control method's capability to migrate between them. The control rule addresses the stabilization of each orbit during 300 forcing period cycles, starting with the period-2, followed by the period-3, and finally the period-1 UPOs.

Figure 6.10 presents the control rule results for the conventional approach with a scalar K. Figure 6.10(a) presents the desired behavior in magenta and the system response in black, while Figure 6.10(b) displays the corresponding control signal. Results are shown over time but exclusively feature the points of the Poincaré map. Results show that the scalar strategy successfully stabilizes the 3 UPOs in the sequence defined by the control rule. The gains used for stabilizing were $R = 0.2$, $K_{22} = 1.2$ for period-2; $R = 0.0$, $K_{22} = 1.9$ for period-1; $R = 0.2$, $K_{22} = 0.6$ for period-3.

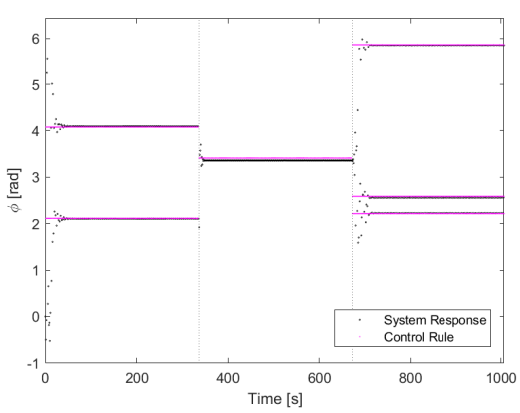

(a) Signal in time.

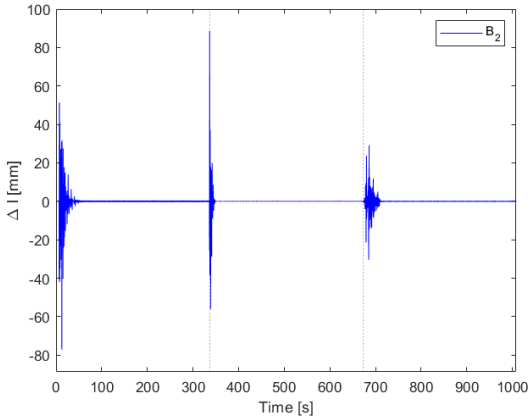

(b) Control signal in time.

Figure 6.10 – Control rules with a scalar K.

Figure 6.11 shows the results for a different control rule when using both K_{21} and K_{22}. The control rule addresses the stabilization of each orbit during 300 forcing period cycles, but now starting with the period-2, followed by the period-1, and finally the period-3 UPOs. Although this strategy stabilized period-2 and period-3 UPOs it was not able to stabilize the desired period-1 UPO, stabilizing a period-3 orbit instead. The gains used for stabilizing were $R = 0.2$, $K_{21} = 0.7$, $K_{22} = 1.2$ for period-2; $R = 0.0$, $K_{21} = 0.2$, $K_{22} = 1.7$ for period-1; $R = 0.2$, $K_{21} = 0.4$, $K_{22} = 0.6$ for period-3.

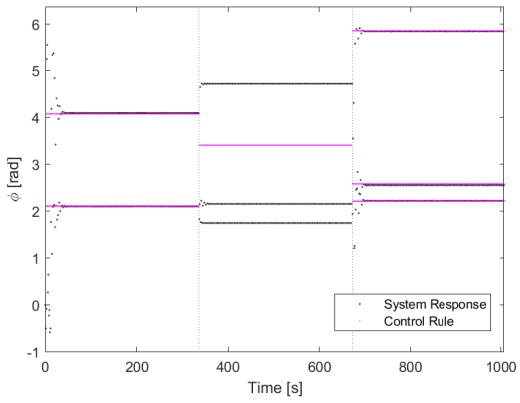

(a) Signal in time.

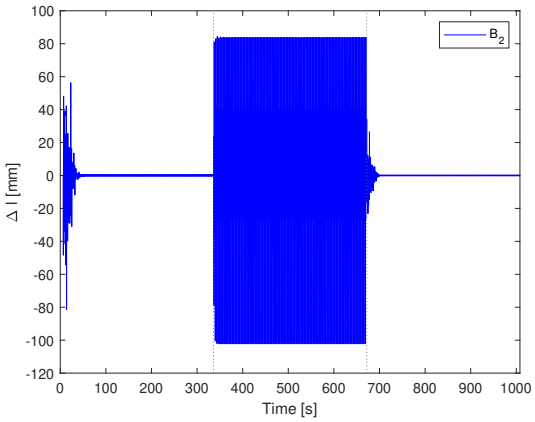

(b) Control signal in time.

Figure 6.11 – Control rules with K_{21} and K_{22}.

Figure 6.12 shows the results for the same previous control rule when using both K_{11} and K_{22}. The control was successful in stabilizing all UPO and migrating between them in the control rules. The gains used for stabilizing were $R = 0.2$, $K_{11} = 0.2$, $K_{22} = 1.0$ for period-2; $R = 0.0$, $K_{11} = 0.2$, $K_{22} = 1.8$ for period-1; $R = 0.2$, $K_{11} = 0.4$, $K_{22} = 0.4$ for period-3.

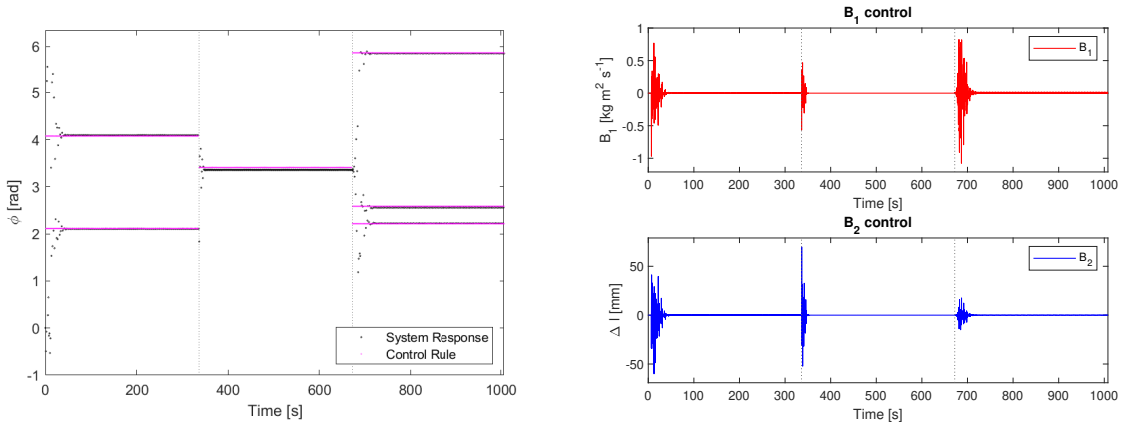

(a) Signal in time. (b) Control signal in time.

Figure 6.12 – Control rules with K_{11} and K_{22}.

The strategy with K_{11}, K_{21} and K_{22} gains is now used to perform the control rule. Similarly to K_{21} and K_{22} case, the control was unsuccessful in stabilizing the period-1 orbit but stabilized a period-3 orbit instead. This suggests that K_{21} gain posed challenges in stabilizing the period-1 orbit. The gains used for stabilizing were $R = 0.2$, $K_{11} = 0.4$, $K_{21} = 0.4$, $K_{22} = 0.8$ for period-2; $R = 0.0$, $K_{11} = 0.2$, $K_{21} = 0.2$, $K_{22} = 1.4$ for period-1; $R = 0.2$, $K_{11} = 0.2$, $K_{21} = 0.4$, $K_{22} = 0.6$ for period-3.

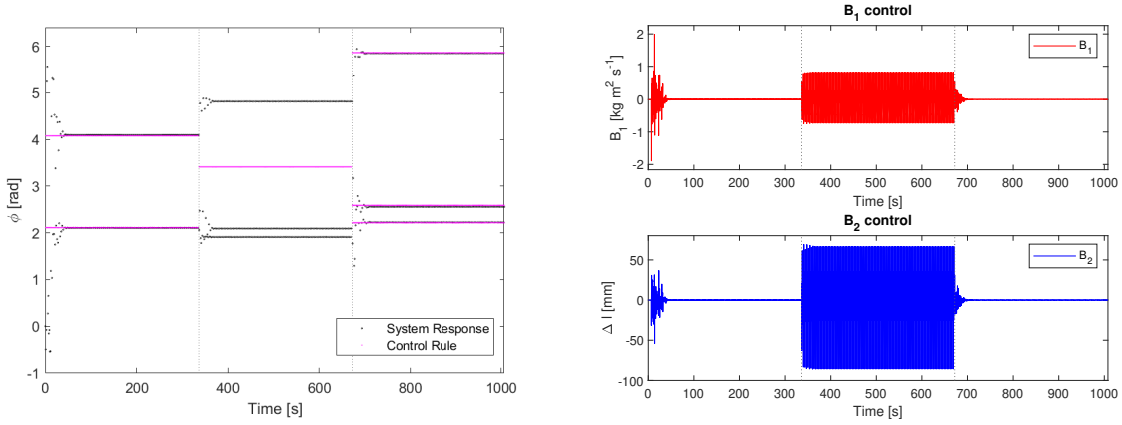

(a) Signal in time. (b) Control signal in time.

Figure 6.13 – Control rules with K_{11}, K_{21}, and K_{22}.

When considering K_{11}, K_{21} and K_{22} simultaneously the stabilization consumed less energy for period-2 and period-3 UPOs. The actuations were significantly smaller for all cases. Higher periodicity orbits had a tendency to consume less energy related to B_2 and higher energy to B_1.

6.5.1 Concluding remarks

System migration between different UPOs was successful achieved in the control without K_{22} gain. In all cases with K_{22} gain, when decreasing the periodicity of the orbit,

the control suppressed the chaotic behavior but stabilized a higher periodicity UPO. Table 6 shows the energy to stabilize each orbit in the control rule.

Control Rule	**Period**	**Energy B1 [J]**	**Energy B2 [J]**	**Energy Total [J]**
K_{22}	2		50.2E+0	50.2E+0
	1		19.6E+0	19.6E+0
	3		30.4E+0	30.4E+0
K_{21}; K_{22}	2		64.6E+0	64.6E+0
	1		1.5E+3	1.5E+3
	3		26.3E+0	26.3E+0
K_{11}; K_{22}	2	34.6E-3	51.5E+0	51.5E+0
	1	17.6E-3	35.1E+0	35.1E+0
	3	65.2E-3	19.0E+0	19.1E+0
K_{11}; K_{21}; K_{22}	2	73.6E-3	43.9E+0	44.0E+0
	1	844.3E-3	1.2E+3	1.2E+3
	3	24.7E-3	23.6E+0	23.6E+0

Table 6 – Comparison of control performance for different sets of control rules.

7 CONCLUSION

This study presents and analyses a generalization of the Extended Time-Delayed Feedback incorporating multiple terms of the gain matrix **K** for controlling chaos in a nonlinear pendulum.

Initially, the work presents a bibliography review that provides an overview of the background and context of chaos control techniques. The review also highlights the limitations of existing methods and the need for new approaches to control chaos in complex systems.

Several authors have previously analyzed the nonlinear pendulum system studied in this dissertation, and its chaotic behavior has been well-documented. The mathematical modeling of the system without control has been evaluated numerically, providing a general overview of its dynamics. Based on this initial analysis, a specific chaotic response is selected to assess the effectiveness of the control procedures.

The learning stage is executed by identifying UPOs and using the maximum Lyapunov exponents to assess the stability of these orbits. This assessment is then employed to define the gains of the controller. The Lyapunov exponents evaluation is the most computationally expensive part of the chaos control. The use of multiple gains in the **K** matrix causes the computational cost to be greater than in the strategy with a scalar.

During the learning stage, 15 UPOs from periods 1 to 6 were identified, among which three were selected for stabilization. Gain K_{12} increased the Lyapunov exponents for all UPOs evaluated, making them more unstable. Thus, this control gain was not considered for control purposes. The maximum Lyapunov exponents calculation using the complete matrix **K** revealed a larger region of negative values for the exponent when compared with the case with a scalar gain K. A larger area of negative Lyapunov exponent increases the number of possibilities for successful control, making it more versatile. In terms of the magnitude of the maximum Lyapunov exponent, consistent orders of magnitude were observed for all cases, with no discernible trends associated with control gains. Therefore, it appears that this parameter may not be the most suitable criterion for determining the best set of control gains.

Maximum actuation and energy consumption required to stabilize the selected orbits were considered as comparison criteria for the stabilization stage. Most cases with

generalized ETDF were able to reduce the maximum actuation when compared to the scalar baseline. The control with three gains in the **K** matrix consistently exhibited lower actuation levels across all tests. When considering two gains in the matrix **K** for the stabilization of Period-1 and Period-3 orbits, the magnitude of the actuation was slightly smaller than that of the scalar baseline. Among all cases, only the stabilization of the Period-2 UPO with both K_{21} and K_{22} exhibited a higher maximum actuation in comparison to the baseline control. This is the result of high values of K_{21} for period-2 orbit.

Regarding energy consumption, the results were dependent on the UPO and the control strategy. Control using both K_{21} and K_{22} was successful in reducing consumption in period-1 and period-3 approaches. In the case of the period-2 UPO, the choice of a high value of K_{21} gain soared control energy consumption, similarly to actuation. Contrary to the actuation magnitude, when using both K_{11} and K_{22}, the energy consumption had the same order of magnitude for most orbits, reducing it only in period-1 UPO. Control strategy considering three gains in **K** matrix decreased consumption in both period-2 and period-3 UPOs, achieving about have of the baseline consumption in period-3.

The control strategy's ability to transition between orbits provides flexibility in chaos control. This capability was evaluated using a control rule associated with the sequential stabilization of three different UPOs, performed by each set of adopted control gains. All strategies without K_{21} gain were successful in orbit migration. In the cases where K_{21} gain was considered, the control method was not able to stabilize the period-1 UPO in the sequential stabilization, making the system trajectory falls in a period-3 orbit instead. This difficulty of stabilizing the period-1 UPO can possibly be solved by selecting an appropriate time, linked to the system state, to activate the control.

The generalization of Extended Time-Delayed Feedback was effective in stabilizing the investigated unstable periodic orbits. The method is more versatile than the scalar approach. It has a wider range of negative Lyapunov values, which implies more possibilities for effective control. The use of multiple gains for control gains allows the choice of those that are most suitable for the real problem, prioritizing reduction of energy consumption or maximum actuation of the system.

For future work, it is proposed to investigate the use of the K_{12} gain to increase the system's instability and facilitate migration between orbits. Furthermore, it is proposed to investigate the generalized ETDF utilizing 0–1 test instead of Lyapunov exponents due to reduced computational expense. Finally, the utilization of machine learning techniques for the learning stage is proposed.

Bibliography

ABEL, A.; SCHWARZ, W. Chaos communications-principles, schemes, and system analysis. *Proceedings of the IEEE*, IEEE, v. 90, n. 5, p. 691–710, 2002. Quoted on page 2.

ALASTY, A.; SALARIEH, H. Controlling the chaos using fuzzy estimation of ogy and pyragas controllers. *Chaos, Solitons & Fractals*, Elsevier, v. 26, n. 2, p. 379–392, 2005. Quoted on page 8.

ARGYRIS, A. et al. Chaos-based communications at high bit rates using commercial fibre-optic links. *Nature*, Nature Publishing Group UK London, v. 438, n. 7066, p. 343–346, 2005. Quoted on page 3.

AUERBACH, D. et al. Exploring chaotic motion through periodic orbits. *Phys. Rev. Lett.*, American Physical Society, v. 58, p. 2387–2389, Jun 1987. Disponível em: <https://link.aps.org/doi/10.1103/PhysRevLett.58.2387>. Quoted 2 times on pages 11 and 15.

AUERBACH, D. et al. Exploring chaotic motion through periodic orbits. *Physical Review Letters*, APS, v. 58, n. 23, p. 2387, 1987. Quoted on page 27.

BARBOSA, W. et al. Chaos control applied to piezoelectric vibration-based energy harvesting systems. *The European Physical Journal Special Topics*, Springer, v. 224, n. 14-15, p. 2787–2801, 2015. Quoted on page 3.

BARRETO, E.; GREBOGI, C. Multiparameter control of chaos. *Physical Review E*, APS, v. 52, n. 4, p. 3553, 1995. Quoted on page 8.

BAYLY, P. V.; VIRGIN, L. N. Practical considerations in the control of chaos. *Physical Review E*, APS, v. 50, n. 1, p. 604, 1994. Quoted on page 7.

BESSA, W. M. et al. Chaos control using an adaptive fuzzy sliding mode controller with application to a nonlinear pendulum. *Chaos, Solitons & Fractals*, Elsevier, v. 42, n. 2, p. 784–791, 2009. Quoted 2 times on pages 3 and 10.

BESSA, W. M. et al. Adaptive fuzzy sliding mode control of a chaotic pendulum with noisy signals. *ZAMM-Journal of Applied Mathematics and Mechanics/Zeitschrift für Angewandte Mathematik und Mechanik*, Wiley Online Library, v. 94, n. 3, p. 256–263, 2014. Quoted on page 3.

BLACKBURN, J. A.; BAKER, G. L. A comparison of commercial chaotic pendulums. *American Journal of Physics*, American Association of Physics Teachers, v. 66, n. 9, p. 821–830, 1998. Quoted 2 times on pages 3 and 21.

BOCCALETTI, S.; ARECCHI, F. Adaptive control of chaos. *Europhysics letters*, IOP Publishing, v. 31, n. 3, p. 127, 1995. Quoted on page 9.

BOCCALETTI, S. et al. The control of chaos: theory and applications. *Physics reports*, Elsevier, v. 329, n. 3, p. 103–197, 2000. Quoted on page 6.

CAI, G.-P.; CHEN, L.-X. Delayed feedback control experiments on some flexible structures. *Acta Mechanica Sinica*, Springer, v. 26, n. 6, p. 951–965, 2010. Quoted on page 8.

CHEN, G.; YU, X. On time-delayed feedback control of chaotic systems. *IEEE Transactions on Circuits and Systems I: Fundamental Theory and Applications*, IEEE, v. 46, n. 6, p. 767–772, 1999. Quoted 2 times on pages 9 and 10.

CHEN, G.; YU, X. *Chaos control: theory and applications*. [S.l.]: Springer Science & Business Media, 2003. v. 292. Quoted on page 3.

CHRISTINI, D. J. et al. Experimental control of high-dimensional chaos: The driven double pendulum. *Physical Review E*, APS, v. 54, n. 5, p. 4824, 1996. Quoted on page 7.

CHRISTINI, D. J. et al. Real-time experimental control of a system in its chaotic and nonchaotic regimes. *Physical Review E*, APS, v. 56, n. 4, p. R3749, 1997. Quoted on page 8.

COSTA, D. D.; SAVI, M. A. Nonlinear dynamics of an sma-pendulum system. *Nonlinear Dynamics*, Springer, v. 87, p. 1617–1627, 2017. Quoted on page 3.

COSTA, D. D.; SAVI, M. A. Chaos control of an sma–pendulum system using thermal actuation with extended time-delayed feedback approach. *Nonlinear Dynamics*, Springer, v. 93, n. 2, p. 571–583, 2018. Quoted on page 3.

DEHGHANI, R.; KHANLO, H. Radial basis function neural network chaos control of a piezomagnetoelastic energy harvesting system. *Journal of Vibration and Control*, SAGE Publications Sage UK: London, England, v. 25, n. 16, p. 2191–2203, 2019. Quoted on page 3.

DESERIO, R. Chaotic pendulum: The complete attractor. *American Journal of Physics*, American Association of Physics Teachers, v. 71, n. 3, p. 250–257, 2003. Quoted on page 3.

DEVANEY, R. L. *Chaos, fractals, and dynamics: computer experiments in mathematics*. [S.l.]: Addison-Wesley Longman Publishing Co., Inc., 1990. Quoted on page 5.

DING, J.; LEI, Y. Control of chaos with time-delayed feedback based on deep reinforcement learning. *Physica D: Nonlinear Phenomena*, Elsevier, v. 451, p. 133767, 2023. Quoted on page 9.

DITTO, W. L. et al. Experimental control of chaos. *Physical Review Letters*, APS, v. 65, n. 26, p. 3211, 1990. Quoted on page 7.

DITTO, W. L. et al. Techniques for the control of chaos. *Physica D: Nonlinear Phenomena*, Elsevier, v. 86, n. 1-2, p. 198–211, 1995. Quoted on page 6.

DRESSLER, U.; NITSCHE, G. Controlling chaos using time delay coordinates. *Physical Review Letters*, APS, v. 68, n. 1, p. 1, 1992. Quoted on page 7.

ECKMANN, J.-P.; RUELLE, D. Ergodic theory of chaos and strange attractors. In: *The theory of chaotic attractors*. [S.l.]: Springer, 1985. p. 273–312. Quoted on page 15.

FARMER, J. D. Chaotic attractors of an infinite-dimensional dynamical system. *Physica D: Nonlinear Phenomena*, Elsevier, v. 4, n. 3, p. 366–393, 1982. Quoted on page 20.

FEIGENBAUM, M. J. Universal behavior in nonlinear systems. *Universality in chaos*, CRC Press, p. 49–84, 1980. Quoted on page 5.

FENG, J. et al. A novel chaos optimization algorithm. *Multimedia Tools and Applications*, Springer, v. 76, p. 17405–17436, 2017. Quoted on page 3.

FERREIRA, B. B. et al. Chaos control applied to cardiac rhythms represented by ecg signals. *Physica Scripta*, IOP Publishing, v. 89, n. 10, p. 105203, 2014. Quoted 2 times on pages 2 and 3.

FRANCA, L. F. P.; SAVI, M. A. Distinguishing periodic and chaotic time series obtained from an experimental nonlinear pendulum. *Nonlinear Dynamics*, Springer, v. 26, n. 3, p. 255–273, 2001. Quoted 2 times on pages 3 and 21.

GALVANETTO, U. Delayed feedback control of chaotic systems with dry friction. *International Journal of Bifurcation and Chaos*, World Scientific, v. 12, n. 08, p. 1877–1883, 2002. Quoted on page 8.

GARFINKEL, A. et al. Controlling cardiac chaos. *Science*, American Association for the Advancement of Science, v. 257, n. 5074, p. 1230–1235, 1992. Quoted 2 times on pages 2 and 3.

GIBB, B. C. Teetering towards chaos and complexity. *Nature Chemistry*, Nature Publishing Group UK London, v. 1, n. 1, p. 17–18, 2009. Quoted on page 2.

GLUCKMAN, B. J. et al. Tracking unstable periodic orbits in nonstationary high-dimensional chaotic systems: method and experiment. *Physical Review E*, APS, v. 55, n. 5, p. 4935, 1997. Quoted on page 7.

GREBOGI, C.; LAI, Y.-C. Controlling chaotic dynamical systems. *Systems & control letters*, Elsevier, v. 31, n. 5, p. 307–312, 1997. Quoted on page 6.

GREBOGI, C. et al. Strange attractors that are not chaotic. *Physica D: Nonlinear Phenomena*, Elsevier, v. 13, n. 1-2, p. 261–268, 1984. Quoted on page 13.

GU, D. et al. Solid-liquid mixing performance in a stirred tank with a double punched rigid-flexible impeller coupled with a chaotic motor. *Chemical Engineering and Processing: Process Intensification*, Elsevier, v. 118, p. 37–46, 2017. Quoted on page 3.

GUNARATNE, G. H. et al. Chaos beyond onset: A comparison of theory and experiment. *Physical Review Letters*, APS, v. 63, n. 1, p. 1, 1989. Quoted on page 15.

HASTINGS, A. et al. Chaos in ecology: is mother nature a strange attractor? *Annual review of ecology and systematics*, Annual Reviews 4139 El Camino Way, PO Box 10139, Palo Alto, CA 94303-0139, USA, v. 24, n. 1, p. 1–33, 1993. Quoted on page 2.

HERRMANN, G. A robust delay adaptation scheme for pyragas' chaos control method. *Physics Letters A*, Elsevier, v. 287, n. 3-4, p. 245–256, 2001. Quoted on page 9.

HIKIHARA, T.; KAWAGOSHI, T. An experimental study on stabilization of unstable periodic motion in magneto-elastic chaos. *Physics Letters A*, Elsevier, v. 211, n. 1, p. 29–36, 1996. Quoted on page 8.

HÖHNE, K. et al. Global properties in an experimental realization of time-delayed feedback control with an unstable control loop. *Physical review letters*, APS, v. 98, n. 21, p. 214102, 2007. Quoted on page 9.

HOOTON, E. W.; AMANN, A. Analytical limitation for time-delayed feedback control in autonomous systems. *Physical Review Letters*, APS, v. 109, n. 15, p. 154101, 2012. Quoted on page 9.

HÜBINGER, B. et al. Controlling chaos experimentally in systems exhibiting large effective lyapunov exponents. *Physical Review E*, APS, v. 50, n. 2, p. 932, 1994. Quoted on page 7.

JUST, W. et al. Mechanism of time-delayed feedback control. *Physical Review Letters*, APS, v. 78, n. 2, p. 203, 1997. Quoted on page 9.

KING, G.; STEWART, I. *Symmetric chaos*. [S.l.]: Academic Press New York, 1991. Quoted on page 2.

KITTEL, A. et al. Delayed feedback control of chaos by self-adapted delay time. *Physics Letters A*, Elsevier, v. 198, n. 5-6, p. 433–436, 1995. Quoted on page 19.

KITTEL, A. et al. Prerecorded history of a system as an experimental tool to control chaos. *Physical Review E*, APS, v. 50, n. 1, p. 262, 1994. Quoted on page 19.

KORTE, R. J. de et al. Experimental control of a chaotic pendulum with unknown dynamics using delay coordinates. *Physical Review E*, APS, v. 52, n. 4, p. 3358, 1995. Quoted on page 7.

KUMAR, A. et al. Enhanced energy harvesting from nonlinear oscillators via chaos control. *IFAC-PapersOnLine*, Elsevier, v. 49, n. 1, p. 35–40, 2016. Quoted on page 3.

LASKAR, J. et al. Strong chaos induced by close encounters with ceres and vesta. *Astronomy & Astrophysics*, EDP Sciences, v. 532, p. L4, 2011. Quoted on page 2.

LECAR, M. et al. Chaos in the solar system. *Annual Review of Astronomy and Astrophysics*, Annual Reviews 4139 El Camino Way, PO Box 10139, Palo Alto, CA 94303-0139, USA, v. 39, n. 1, p. 581–631, 2001. Quoted on page 2.

LEHNERT, J. et al. Adaptive tuning of feedback gain in time-delayed feedback control. *Chaos: An Interdisciplinary Journal of Nonlinear Science*, AIP Publishing, v. 21, n. 4, 2011. Quoted on page 9.

LEINE, R. I. Bifurcations in discontinuous mechanical systems of the fillippov-type. 2000. Quoted on page 23.

LEONOV, G. A. Pyragas stabilizability via delayed feedback with periodic control gain. *Systems & Control Letters*, Elsevier, v. 69, p. 34–37, 2014. Quoted on page 9.

LI, L. et al. An optimization method inspired by" chaotic" ant behavior. *International Journal of Bifurcation and Chaos*, World Scientific, v. 16, n. 08, p. 2351–2364, 2006. Quoted on page 3.

LINDNER, J. F.; DITTO, W. L. Removal, suppression, and control of chaos by nonlinear design. 1995. Quoted on page 2.

LINSAY, P. S. Period doubling and chaotic behavior in a driven anharmonic oscillator. *Physical review letters*, APS, v. 47, n. 19, p. 1349, 1981. Quoted on page 5.

LITAK, G. et al. Chaotic vibration of a quarter-car model excited by the road surface profile. *Communications in Nonlinear Science and Numerical Simulation*, Elsevier, v. 13, n. 7, p. 1373–1383, 2008. Quoted on page 3.

LIU, C.-X. et al. Resonance and chaos of micro and nano electro mechanical resonators with time delay feedback. *Applied Mathematical Modelling*, Elsevier, v. 79, p. 469–489, 2020. Quoted on page 8.

LORENZ, E. N. Deterministic nonperiodic flow. *Journal of atmospheric sciences*, v. 20, n. 2, p. 130–141, 1963. Quoted 2 times on pages 2 and 5.

LOUNIS, F. et al. Implementing high-order chaos control scheme for cardiac conduction model with pathological rhythms. *Chaos, Solitons & Fractals*, Elsevier, v. 132, p. 109581, 2020. Quoted 2 times on pages 2 and 3.

MANDELBROT, B. B.; MANDELBROT, B. B. *The fractal geometry of nature*. [S.l.]: WH freeman New York, 1982. v. 1. Quoted on page 5.

MAY, R. M. Simple mathematical models with very complicated dynamics. *Nature*, Nature Publishing Group UK London, v. 261, n. 5560, p. 459–467, 1976. Quoted on page 5.

MOHAMMADPOUR, M. et al. Controlling chaos in bi-stable energy harvesting systems using delayed feedback control. *Meccanica*, Springer, p. 1–20, 2023. Quoted on page 3.

MOON, F.; HOLMES, P. J. A magnetoelastic strange attractor. *Journal of Sound and Vibration*, Elsevier, v. 65, n. 2, p. 275–296, 1979. Quoted on page 5.

MOON, F. C. Chaotic and fractal dynamics—an introduction for applied scientists and engineers john wiley & sons. *Inc., New York*, 1992. Quoted 2 times on pages x and 12.

NAKAJIMA, H. On analytical properties of delayed feedback control of chaos. *Physics Letters A*, Elsevier, v. 232, n. 3-4, p. 207–210, 1997. Quoted on page 9.

NAKAJIMA, H.; UEDA, Y. Half-period delayed feedback control for dynamical systems with symmetries. *Physical review E*, APS, v. 58, n. 2, p. 1757, 1998. Quoted on page 9.

NAKAJIMA, H.; UEDA, Y. Limitation of generalized delayed feedback control. *Physica D: Nonlinear Phenomena*, Elsevier, v. 111, n. 1-4, p. 143–150, 1998. Quoted on page 9.

NAZZAL, J. M.; NATSHEH, A. N. Chaos control using sliding-mode theory. *Chaos, Solitons & Fractals*, Elsevier, v. 33, n. 2, p. 695–702, 2007. Quoted on page 10.

OLSEN, L. F.; DEGN, H. Chaos in an enzyme reaction. *Nature*, Nature Publishing Group UK London, v. 267, n. 5607, p. 177–178, 1977. Quoted on page 5.

OTANI, M.; JONES, A. J. Guiding chaotic orbits. *Research Report, Imperial College of Science Technology and Medicine*, v. 130, 1997. Quoted 2 times on pages 5 and 11.

OTT, E. et al. Controlling chaos. *Physical review letters*, APS, v. 64, n. 11, p. 1196, 1990. Quoted 2 times on pages 3 and 6.

PARKER, T. S.; CHUA, L. *Practical numerical algorithms for chaotic systems*. [S.l.]: Springer Science & Business Media, 2012. Quoted on page 14.

PAULA, A. D. Caos em sistemas mecânicos: Análise experimental em um pêndulo não-linear. *Projeto de fim de curso, Universidade Federal do Rio de Janeiro*, 2005. Quoted 2 times on pages x and 24.

PAULA, A. S. D. Controle de caos em sistemas mecânicos. *Rio de Janeiro, Rio de Janeiro, Brasil: Tese (Doutorado)-UFRJ/COPPE*, 2010. Quoted on page 21.

PAULA, A. S. D.; SAVI, M. A. Comparative analysis of chaos control methods: A mechanical system case study. *International Journal of Non-Linear Mechanics*, Elsevier, v. 46, n. 8, p. 1076–1089, 2011. Quoted 5 times on pages 3, 6, 18, 29, and 44.

PAULA, A. S. de; SAVI, M. A. Controlling chaos in a nonlinear pendulum using an extended time-delayed feedback control method. *Chaos, Solitons & Fractals*, Elsevier, v. 42, n. 5, p. 2981–2988, 2009. Quoted 4 times on pages 3, 9, 29, and 44.

PAULA, A. S. de; SAVI, M. A. A multiparameter chaos control method based on ogy approach. *Chaos, Solitons & Fractals*, Elsevier, v. 40, n. 3, p. 1376–1390, 2009. Quoted on page 8.

PAULA, A. S. de; SAVI, M. A. State space reconstruction applied to a multiparameter chaos control method. *Meccanica*, Springer, v. 50, p. 207–216, 2015. Quoted on page 3.

PAULA, A. S. de et al. Chaos and transient chaos in an experimental nonlinear pendulum. *Journal of sound and vibration*, Elsevier, v. 294, n. 3, p. 585–595, 2006. Quoted 4 times on pages 3, 21, 22, and 23.

PEREIRA-PINTO, F. H. I. et al. Chaos control in a nonlinear pendulum using a semi-continuous method. *Chaos, Solitons & Fractals*, Elsevier, v. 22, n. 3, p. 653–668, 2004. Quoted 2 times on pages 3 and 13.

PINTO, E. G.; SAVI, M. A. Nonlinear prediction of time series obtained from an experimental pendulum. *Current Topics in Acoustical Research*, v. 3, p. 151–162, 2003. Quoted 2 times on pages 3 and 21.

POINCARÉ, H. Sur le problème des trois corps et les équations de la dynamique. *Acta mathematica*, Springer Netherlands, v. 13, n. 1, p. A3–A270, 1890. Quoted on page 5.

PYRAGAS, K. Continuous control of chaos by self-controlling feedback. *Physics letters A*, Elsevier, v. 170, n. 6, p. 421–428, 1992. Quoted 5 times on pages 3, 6, 8, 9, and 18.

PYRAGAS, K. Control of chaos via extended delay feedback. *Physics letters A*, Elsevier, v. 206, n. 5-6, p. 323–330, 1995. Quoted 4 times on pages 17, 19, 20, and 29.

PYRAGAS, K. Control of chaos via an unstable delayed feedback controller. *Physical Review Letters*, APS, v. 86, n. 11, p. 2265, 2001. Quoted on page 9.

PYRAGAS, K. Delayed feedback control of chaos. *Philosophical Transactions of the Royal Society A: Mathematical, Physical and Engineering Sciences*, The Royal Society London, v. 364, n. 1846, p. 2309–2334, 2006. Quoted 2 times on pages 6 and 9.

PYRAGAS, K.; TAMAŠEVIČIUS, A. Experimental control of chaos by delayed self-controlling feedback. *Physics Letters A*, Elsevier, v. 180, n. 1-2, p. 99–102, 1993. Quoted 2 times on pages 8 and 9.

PYRAGAS, V.; PYRAGAS, K. Act-and-wait time-delayed feedback control of nonautonomous systems. *Physical Review E*, APS, v. 94, n. 1, p. 012201, 2016. Quoted on page 9.

PYRAGAS, V.; PYRAGAS, K. Act-and-wait time-delayed feedback control of autonomous systems. *Physics Letters A*, Elsevier, v. 382, n. 8, p. 574–580, 2018. Quoted on page 9.

QUEIROZ, A. R. et al. Chaos control in a nonlinear pendulum using a generalized extended time-delayed feedback method. *DINAME 2023 - XIX International Symposium on Dynamic Problems of Mechanics*, Associação Brasileira de Engenharia e Ciências Mecânicas, 2023. Quoted on page 3.

RAMESH, M.; NARAYANAN, S. Controlling chaotic motions in a two-dimensional airfoil using time-delayed feedback. *Journal of sound and Vibration*, Elsevier, v. 239, n. 5, p. 1037–1049, 2001. Quoted on page 8.

RITZ, T. et al. Chaos control with adjustable control times. *Chaos, Solitons & Fractals*, Elsevier, v. 8, n. 9, p. 1559–1576, 1997. Quoted on page 8.

ROMEIRAS, F. J. et al. Controlling chaotic dynamical systems. *Physica D: Nonlinear Phenomena*, Elsevier, v. 58, n. 1-4, p. 165–192, 1992. Quoted on page 7.

RÖSSLER, O. E. Chaos and chemistry. In: SPRINGER. *Nonlinear Phenomena in Chemical Dynamics: Proceedings of an International Conference, Bordeaux, France, September 7–11, 1981*. [S.l.], 1981. p. 79–87. Quoted on page 2.

ROUX, J.-C. et al. Observation of a strange attractor. *Physica D: Nonlinear Phenomena*, Elsevier, v. 8, n. 1-2, p. 257–266, 1983. Quoted on page 5.

RUELLE, D.; TAKENS, F. On the nature of turbulence. *Les rencontres physiciens-mathématiciens de Strasbourg-RCP25*, v. 12, p. 1–44, 1971. Quoted on page 5.

SAVI, M. A. *Dinâmica não-linear e caos*. [S.l.]: Editora E-papers, 2006. Quoted 5 times on pages 3, 11, 13, 16, and 17.

SAVI, M. A. et al. Chaos control in mechanical systems. *Shock and Vibration*, IOS Press, v. 13, n. 4-5, p. 301–314, 2006. Quoted on page 6.

SCHÖLL, E.; SCHUSTER, H. G. Handbook of chaos control. Wiley Online Library, 2008. Quoted 2 times on pages 2 and 6.

SHAW, S. W.; RAND, R. H. The transition to chaos in a simple mechanical system. *International Journal of Non-Linear Mechanics*, Elsevier, v. 24, n. 1, p. 41–56, 1989. Quoted on page 2.

SKINNER, J. E. et al. Application of chaos theory to biology and medicine. *Integrative Physiological and Behavioral Science*, Springer, v. 27, p. 39–53, 1992. Quoted on page 2.

SO, P.; OTT, E. Controlling chaos using time delay coordinates via stabilization of periodic orbits. *Physical Review E*, APS, v. 51, n. 4, p. 2955, 1995. Quoted on page 7.

SOCOLAR, J. E. et al. Stabilizing unstable periodic orbits in fast dynamical systems. *Physical Review E*, APS, v. 50, n. 4, p. 3245, 1994. Quoted 2 times on pages 3 and 9.

SPROTT, J. A simple chaotic delay differential equation. *Physics Letters A*, Elsevier, v. 366, n. 4-5, p. 397–402, 2007. Quoted on page 20.

SUGIMOTO, Y.; OSUKA, K. Walking control of quasi passive dynamic walking robot" quartet iii" based on continuous delayed feedback control. In: IEEE. *2004 IEEE International Conference on Robotics and Biomimetics*. [S.l.], 2004. p. 606–611. Quoted on page 8.

SWINNEY, H. L.; GOLLUB, J. P. Hydrodynamic instabilities and the transition to turbulence. *Hydrodynamic instabilities and the transition to turbulence*, 1981. Quoted on page 5.

TAN, T. et al. Piezoelectric autoparametric vibration energy harvesting with chaos control feature. *Mechanical Systems and Signal Processing*, Elsevier, v. 161, p. 107989, 2021. Quoted on page 3.

TIAN, L. et al. On a new time-delayed feedback control of chaotic systems. *Chaos, Solitons & Fractals*, Elsevier, v. 39, n. 2, p. 831–839, 2009. Quoted on page 9.

TIAN, Y.-P.; YU, X. Stabilizing unstable periodic orbits of chaotic systems via an optimal principle. *Journal of the Franklin Institute*, Elsevier, v. 337, n. 6, p. 771–779, 2000. Quoted on page 10.

TSAI, H.-H. et al. A robust controller for chaotic systems under external excitation. *Chaos, Solitons & Fractals*, Elsevier, v. 14, n. 4, p. 627–632, 2002. Quoted on page 10.

USHIO, T. Limitation of delayed feedback control in nonlinear discrete-time systems. *IEEE Transactions on Circuits and Systems I: Fundamental Theory and Applications*, IEEE, v. 43, n. 9, p. 815–816, 1996. Quoted on page 9.

USHIO, T.; YAMAMOTO, S. Delayed feedback control with nonlinear estimation in chaotic discrete-time systems. *Physics Letters A*, Elsevier, v. 247, n. 1-2, p. 112–118, 1998. Quoted on page 9.

USHIO, T.; YAMAMOTO, S. Prediction-based control of chaos. *Physics Letters A*, Elsevier, v. 264, n. 1, p. 30–35, 1999. Quoted on page 9.

VICENTE, R. et al. Analysis and characterization of the hyperchaos generated by a semiconductor laser subject to a delayed feedback loop. *IEEE Journal of Quantum Electronics*, IEEE, v. 41, n. 4, p. 541–548, 2005. Quoted on page 19.

VIEIRA, M. de S.; LICHTENBERG, A. J. Controlling chaos using nonlinear feedback with delay. *Physical Review E*, APS, v. 54, n. 2, p. 1200, 1996. Quoted on page 10.

WANG, X. F. et al. Anticontrol of chaos in continuous-time systems via time-delay feedback. *Chaos: An Interdisciplinary Journal of Nonlinear Science*, American Institute of Physics, v. 10, n. 4, p. 771–779, 2000. Quoted on page 10.

WANG, Z.; CHAU, K. Anti-control of chaos of a permanent magnet dc motor system for vibratory compactors. *Chaos, Solitons & Fractals*, Elsevier, v. 36, n. 3, p. 694–708, 2008. Quoted 2 times on pages 3 and 10.

WEI, H. et al. Controlling chaos by a delayed continuous feedback in a gas discharge plasma. *Chinese Physics*, IOP Publishing, v. 13, n. 11, p. 1913, 2004. Quoted on page 8.

WEST, B. J. *Fractal physiology and chaos in medicine*. [S.l.]: World Scientific, 2012. v. 16. Quoted on page 2.

WOLF, A. et al. Determining lyapunov exponents from a time series. *Physica D: Nonlinear Phenomena*, Elsevier, v. 16, n. 3, p. 285–317, 1985. Quoted 3 times on pages 16, 17, and 20.

WORSTER, D. The ecology of order and chaos. *Environmental History Review*, The University of Chicago Press, v. 14, n. 1-2, p. 1–18, 1990. Quoted on page 2.

XU, D. et al. Estimation of periodic-like motions of chaotic evolutions using detected unstable periodic patterns. *Pattern Recognition Letters*, Elsevier, v. 23, n. 1-3, p. 245–252, 2002. Quoted on page 15.

YAGASAKI, K. Extension of a chaos control method to unstable trajectories on infinite-or finite-time intervals: Experimental verification. *Physics Letters A*, Elsevier, v. 368, n. 3-4, p. 222–226, 2007. Quoted on page 8.

YANG, D. et al. On the efficiency of chaos optimization algorithms for global optimization. *Chaos, Solitons & Fractals*, Elsevier, v. 34, n. 4, p. 1366–1375, 2007. Quoted on page 3.

YU, X. et al. An invariant-manifold-based method for chaos control. *IEEE Transactions on Circuits and Systems I: Fundamental Theory and Applications*, IEEE, v. 48, n. 8, p. 930–937, 2001. Quoted on page 8.

ZEEBE, R. E.; LOURENS, L. J. Solar system chaos and the paleocene–eocene boundary age constrained by geology and astronomy. *Science*, American Association for the Advancement of Science, v. 365, n. 6456, p. 926–929, 2019. Quoted on page 2.

ZHOU, Z.-X. et al. Parameter impulse control of chaos in crystal growth process. *Journal of Crystal Growth*, Elsevier, v. 563, p. 126079, 2021. Quoted on page 3.